



HAL
open science

Hydrogen sulfide solubility in 50 wt% and 70 wt% aqueous methyldiethanolamine at temperatures from 283 to 393 K and total pressures from 500 to 10000 kPa

Eirini Skylogianni, Ingvild Mundal, Diego D.D. Pinto, Christophe Coquelet, Hanna Knuutila

► **To cite this version:**

Eirini Skylogianni, Ingvild Mundal, Diego D.D. Pinto, Christophe Coquelet, Hanna Knuutila. Hydrogen sulfide solubility in 50 wt% and 70 wt% aqueous methyldiethanolamine at temperatures from 283 to 393 K and total pressures from 500 to 10000 kPa. *Fluid Phase Equilibria*, 2020, pp.112498. 10.1016/j.fluid.2020.112498 . hal-02463973

HAL Id: hal-02463973

<https://hal.science/hal-02463973>

Submitted on 2 Feb 2020

HAL is a multi-disciplinary open access archive for the deposit and dissemination of scientific research documents, whether they are published or not. The documents may come from teaching and research institutions in France or abroad, or from public or private research centers.

L'archive ouverte pluridisciplinaire **HAL**, est destinée au dépôt et à la diffusion de documents scientifiques de niveau recherche, publiés ou non, émanant des établissements d'enseignement et de recherche français ou étrangers, des laboratoires publics ou privés.

1

2 **Hydrogen Sulfide Solubility in 50 wt.% and 70 wt.% Aqueous**
3 **Methyldiethanolamine at Temperatures from 283 to 393 K and Total**
4 **Pressures from 500 to 10000 kPa**

5

6

7

8 Eirini Skylogianni¹, Ingvild Mundal¹, Diego D.D. Pinto¹, Christophe Coquelet², Hanna

9

K. Knuutila^{*,1}

10

11

12 ¹*Department of Chemical Engineering, Norwegian University of Science and*

13 *Technology, Sem Sælands vei 6, 7034 Trondheim, Norway*

14 ²*Mines ParisTech - PSL University, CTP- Centre of Thermodynamics of Processes,*

15 *35 rue Saint Honoré, 77305 Fontainebleau, France*

16

17

18

19

20

21

22 * Corresponding author. E-mail: hanna.knuutila@ntnu.no

23 **Abstract**

24 The hydrogen sulfide (H₂S) absorption capacity of a 70 wt.% aqueous
25 methyldiethanolamine (MDEA) solution was investigated in a static-analytic apparatus
26 at temperatures of 283, 353 and 393 K and pressures of 2000, 6000 and 10000 kPa in the
27 presence of methane. New experimental data were also produced for a 50.1 wt.% aqueous
28 MDEA at 323 K and pressures of 500 and 3000 kPa as part of the apparatus validation
29 procedure. A model based on electrolyte non-random two-liquid (eNRTL) activity
30 coefficient model to describe the liquid phase and Peng-Robinson Equation of State to
31 describe the vapor phase non-idealities was developed for the system H₂S-MDEA-H₂O,
32 which can potentially be used also for the system in the presence of methane at low
33 pressures. Vapor pressure measurements of pure MDEA were also performed in the range
34 of 405 – 435 K in an ebulliometer and parameters for the Antoine correlation were
35 proposed.

36

37 *Keywords:* gas processing; absorption; hydrogen sulfide; methane; MDEA; high
38 pressure; vapor-liquid equilibrium; vapor pressure

39 1. Introduction

40 Natural and refinery gas streams usually contain acid gases, carbon dioxide and sulfur
41 compounds, which must be removed in order to ensure trouble-free and safe operations.
42 Typical sulfur compounds are hydrogen sulfide, carbonyl sulfide, mercaptans, with the
43 first one being the most important one as it occurs in the largest concentrations [1].
44 Hydrogen sulfide (H₂S) gas content is routinely controlled by absorption into aqueous
45 methyldiethanolamine (MDEA), which can then be thermally regenerated and reused.

46 A 50 wt.% MDEA-H₂O concentration is considered a benchmark solvent in H₂S
47 removal, due to its equilibrium behavior and low corrosion. Aqueous MDEA has been
48 long established in the industry due to among others, the amine's availability, low cost
49 and energy requirements, resistance to degradation, ability to meet the 4 ppm
50 specification requirement for pipeline gas and to selectively remove H₂S over CO₂, which
51 often coexist. MDEA owes its latter characteristic to its structure; as a tertiary amine,
52 aqueous MDEA reacts instantaneously with hydrogen sulfide while it requires more time
53 to react with CO₂. Thus, by regulating the contact time between the solvent and the gas,
54 H₂S removal to specification and minimum co-absorption of CO₂ can be achieved [2],
55 [3].

56 The motivation of this work has been the investigation of highly concentrated MDEA
57 for the combined H₂S removal and hydrate control for subsea application. Oil and gas
58 reservoirs are turning sour in the course of time [4], [5], which is tackled today by using
59 triazine to control the H₂S levels [6]. Main disadvantages of employment of triazine are
60 related to the non-regeneration of the solvent, weight, space, transportation and disposal
61 requirements. These constraints are of utmost importance, especially as the available
62 production fields are sourer, deeper and in longer distances from the shore [7]. MDEA is
63 already used offshore as a pH stabilizer [8] facilitating its employment subsea, while the
64 fact that, as a polar compound, it has affinity for water, renders highly concentrated
65 aqueous MDEA a good candidate for acting both as a hydrate inhibitor and as an H₂S
66 removal agent. The solvent could be used and regenerated offshore, supported by new
67 technological developments, such as "subsea on a stick" [9].

68 This work is a first step in the investigation of this multifunctional solvent, with focus
69 on the effect of total pressure in the H₂S removal capacity of the solvent. The

70 measurements were conducted at high pressures, up to 10000 kPa, with methane as the
71 pressurization medium, since it is the main constituent of natural gas. Few researchers
72 have previously studied the effect of high-pressure methane for the systems CH₄-CO₂-
73 MDEA-H₂O [10], [11] and CH₄-H₂S-MDEA-H₂O; a detailed literature review for the
74 latter is provided in **Section 2.1**. The main finding has been that for both CO₂ and H₂S-
75 contained systems, an increase in total pressure leads to increase in the acid gas partial
76 pressure. To our best knowledge, there are no data reported for the system CH₄-H₂S-
77 MDEA-H₂O and MDEA solutions with concentrations higher than 50 wt.% MDEA-H₂O.

78 A 50.1 wt.% MDEA-H₂O and a 70 wt.% MDEA-H₂O system were used in this work
79 to obtain vapor-liquid equilibrium data (VLE) with hydrogen sulfide and methane. The
80 new VLE data for the system CH₄-H₂S-MDEA-H₂O with 70 wt.% MDEA-H₂O mixtures
81 were obtained at temperatures of approximately 283, 353 and 393 K and pressures of
82 2000, 6000 and 10000 kPa. The experiments were performed isothermally and the
83 temperature of 283 K was chosen to simulate the low-temperature subsea conditions
84 while the temperature of 393 K was chosen to simulate the high regeneration temperature.

85 **2. Literature Review**

86 **2.1 H₂S-MDEA-H₂O-makeup gas system**

87 An updated list of available VLE data for the system H₂S-MDEA-H₂O, including data
88 with makeup gas, is provided in **Table 1**. The amine concentration is expressed in a
89 weight basis for all reference sources to allow for direct comparisons. Concentrations
90 reported in molarities [12]–[14] have been converted to weight fractions using the density
91 correlations presented by Bernal-García et al. [15]. The solution preparation temperature
92 was assumed to be 298.15 K due to lack of this information.

93 As also other authors working with the system H₂S-MDEA-H₂O have observed, the
94 available data in the literature are rather scattered, especially at low loadings. The
95 literature data have been evaluated for self-consistency and mutual-consistency with
96 reported data in similar experimental conditions, following Chunxi and Fürst's approach
97 [16]. This evaluation was performed in order to decide if some data sets would be

98 excluded during our thermodynamic modeling. During the evaluation, the partial
99 pressures for H₂S from Kuranov et al. [17], Kamps et al. [18] and Sidi-Boumedine et al.
100 [19], who all report total pressures in the absence of makeup gases, were calculated by
101 subtracting the vapor pressure of the solvent calculated by Dalton's Law (Eq. 1). The
102 vapor pressure of H₂O was calculated by the correlations proposed by NIST for the given
103 temperature ranges while the vapor pressure of MDEA was calculated based on the
104 Antoine correlation fitted to existing and new data as presented in **Section 5. Results and**
105 **Discussion.**

$$P_{solv}^S = P_{MDEA}^S \cdot x_{MDEA} + P_{H_2O}^S \cdot x_{H_2O} \quad \text{Eq. 1}$$

106

107 Li and Shen [13] measured H₂S solubility in 29.9 wt.% aqueous MDEA at
108 temperatures up to 373 K. During the evaluation of the data, a sharp increase of partial
109 pressure at loadings > 0.7 mol H₂S/mol MDEA was noticed, resulting in a cross-over of
110 literature data reported for 35 wt.% and 50 wt.% MDEA-H₂O solutions. For this reason,
111 the data from Li and Shen [13] were not included in our database used in the model
112 parametrization, as chosen also by Huttenhuis et al. [20].

113 Jou and coworkers [12], [21] have published experimental data for a 48.9 wt.% and
114 for a 35 wt.% MDEA solution. Two observations can be made for the low loading region:
115 a) the data with a 35 wt.% [21] and a 48.9 wt.% [12] MDEA solution are very similar and
116 b) the deviations between the data with a 48.9 wt.% and a 50 wt.% solution look larger
117 than what one would expect with such similar concentrations. Uncertainty information is
118 not given in the first publication of Jou et al. [12], while the authors on their second
119 publication report 3% error in liquid loading and 0.1% full scale (FS) error in pressure.
120 Taking this into account, the deviations related to a) and b) are within the experimental
121 uncertainty. Generally, the data from Jou et al. agree with literature values in different
122 concentrations and temperatures besides at low loadings. For example, good agreement
123 is observed between the data Jou et al. [12] for a 23.4 wt.% aqueous MDEA at 313 K and
124 from two other sources [14], [22] at loadings > 0.4 mol H₂S/mol MDEA. Any small
125 deviations are justified in terms of reported experimental uncertainties provided by
126 MacGregor and Mather [14] (pressure, loading, composition) as well as by Zoghi and
127 Shokouhi [22] (pressure and composition). At lower loadings, significant deviations are

128 seen between the data by Jou et al. [12] and MacGregor and Mather [14] compared to
129 Huang and Ng [23] as well as Rogers et al. [24]. These differences are difficult to explain
130 by the reported uncertainties. At higher loadings, some inconsistencies are also seen, for
131 example, the data from Kuranov and coworkers [17] for a 32.3 wt.% amine solution are
132 close to the data reported for a 50 wt.% MDEA solution [12], [23].

133 No pattern was identified between the analysis method and the uncertainty of the
134 results. Unfortunately, often the uncertainty in loading, which could enlighten the reasons
135 for the scatter observed at low loadings, is not reported. The literature sources reporting
136 uncertainties in either pressure or loading are marked in **Table 1**. In addition, the
137 differences observed in the reported data could also be attributed to the purity of the
138 chemicals. Although most of the authors report the use relatively high-purity chemicals
139 (>98-99 wt.% MDEA, >99 vol.% H₂S), the chemical's aging (contamination, contact with
140 atmospheric humidity, light degradation etc.) could also have contributed to the
141 differences observed.

142 **Table 1.** Literature VLE data for H₂S-MDEA-H₂O including data with makeup gas.

| wt. % aq. MDEA | T (K) | P _{H₂S} (kPa) | P _{tot} (kPa) | Loading | Makeup gas | Analysis Method | | Source | NP |
|------------------|--|-----------------------------------|------------------------|--------------------------|--|---|--|---|-----|
| | | | | | | Vapor Phase | Liquid Phase | | |
| 11.8, 23.4, 48.9 | 298.15, 313.15, 323.15, 373.15, 393.15 | 0.0013-5890 | - | 0.00129-3.229 | Nitrogen (P _{H₂S} < 200 kPa) | GC | Iodometric back-titration with thiosulfate | Jou et al. [12] | 153 |
| 11.9, 20 | 298.15, 310.95, 338.75, 388.75 | 13.23-1536.6 | - | 0.18-2.1703 | - | Mass balance | Mass balance | Bhairi, Maddox et al. [26], [27] ^{+,*} | 49 |
| 23.4 | 313.15 | 0.52-1600 | - | 0.13-1.725 | - | GC | Iodometric back-titration with thiosulfate | MacGregor and Mather [14] ^{+,*} | 27 |
| 35, 50 | 313.15, 373.15 | 0.00183-313 | - | 0.00410-1.077 | Nitrogen (P _{H₂S} < 350 kPa) | GC | Iodometric back-titration with thiosulfate | Jou et al. [21] [*] | 50 |
| 29.9 | 313.15, 333.15, 353.15, 373.15 | 1.498-445.7 | - | 0.082-0.902 | Nitrogen (P _{H₂S} < 200 kPa) | Mass balance (P _{H₂S} < 200 kPa) / GC (P _{H₂S} > 200 kPa) | Iodometric back-titration with thiosulfate | Li and Shen [13] [*] | 43 |
| 23.1, 50 | 313.15, 343.15, 373.15, 393.15 | 0.0033-3673 | - | 0.00240-1.74 | Nitrogen (P _{H₂S} < P _{amb}) | Mass balance | Iodometric back-titration with thiosulfate | Huang and Ng [23] [*] | 42 |
| 23, 50 | 313.15, 323.15 | 0.00069-5.268 | 96-110 | 0.00219-0.313 | Nitrogen (P _{H₂S} < P _{amb}) | FTIR | FTIR | Rogers et al. [24] ^{+,*} | 30 |
| 11.83, 23.63 | ~298.15, ~313.1 | 0.023-1.611 | - | 0.0101-0.2610 | - | Mass balance | Mass balance | Lemoine et al. [28] ^{+,*} | 29 |
| 18.7, 32.2 | 313.16, 333.15, 373.15, 393.15, 413.15 | - | 165.2-4895.9 | 0.48-1.934 | - | Mass balance | Mass balance | Kuranov et al. [17] ^{+,*} | 71 |
| 48.8 | 313.11, 353.16, 393.15 | - | 147.9-2783 | 0.153-1.428 | - | Mass balance | Mass balance | Kamps et al. [18] ^{+,*} | 26 |
| 46.78 | ~ 313, ~373 | - | 6.21-1040 | 0.039-1.116 | - | Mass balance | Mass balance | Sidi-Boumedine et al. [19] ^{+,*} | 27 |
| 23.7 | 313.2 | 14-1361 | - | 0.505-1.639 | - | Mass balance | Mass balance | Zoghi and Shokouhi [22] ^{+,*} | 12 |
| 35, 50 | 283, 298, (313) | 0.141-18.892 | 690-6900 | 0.028-0.575 | Methane | GC | Iodometric back-titration with thiosulfate | Huttenhuis et al. [25] | 30 |
| 50 | 323.15 | 3-278 | 493-700 | 0.096-0.889 ^a | Methane | GC | Mass balance | Dicko et al. [29] ^{+,*} | 5 |
| 50 | 322.95, 343.15 | 31-974 | 1480-7090 | 0.267-1.042 | Methane | GC | Titration with silver nitrate | Sadegh et al. [30] ^{+,*} | 39 |

^a: global loading, ⁺: reported uncertainty in pressure, ^{*}: reported uncertainty in H₂S loading/mole fraction

144

2.2 MDEA-H₂O system

145 Vapor-liquid equilibrium (VLE), freezing-point depression (FPD) and molar excess
 146 enthalpy H^E data for the binary subsystem MDEA-H₂O are given in **Table 2**. The data were
 147 used to model the binary system first in order to reduce the number of parameters to be fitted
 148 for the ternary system H₂S-MDEA-H₂O onwards, as it will be further explained later in **Section**
 149 **4. Thermodynamic modeling**. Eight points from Chang et al. [31] were excluded due to their
 150 deviations from the data by Fosbøl et al. [32]

151 **Table 2.** Literature VLE, FPD and H^E data for the binary system MDEA-H₂O.

| Property | wt.% aq. MDEA | $T / \Delta T_F$ (K) | P (kPa) | Source | NP |
|----------|---------------|----------------------|--------------|---------------------|----|
| VLE | 3-78.61 | 313.15-373.15 | 6.47-100.40 | Kim et al. [33] | 61 |
| | 10-70 | 326.15-381.15 | 13.08-101.67 | Xu et al. [34] | 34 |
| | 30-98.9 | 350.15-458.65 | 40-66.7 | Voutsas et al. [35] | 27 |
| FPD | 17.4-39.1 | (-3.3)-(-13.8) | 101.13 | Chang et al. [31] | 21 |
| | 2.6-39.6 | (-0.4)-(-14.2) | 101.3 | Fosbøl et al. [32] | 12 |
| H^E | 9.6-92.5 | 298.15-342.45 | - | Posey [36] | 16 |
| | 17.5-96.7 | 298.15-313.15 | - | Maham et al. [37] | 26 |
| | 41.8-98.4 | 338.15 | - | Maham et al. [38] | 9 |

152

2.3 Pure MDEA

153 A literature review was also performed for the vapor pressure of MDEA. As seen in **Table 3**,
 154 the data already reported in the literature cover a large range of temperatures, from 293 to 738
 155 K.

156 **Table 3.** Literature vapor pressure data for pure MDEA.

| T (K) | P^s (kPa) | Source | NP |
|------------------------|---------------|------------------------------|----|
| 293.69-401.97 | 0.0006-1.4776 | Noll et al. [39] | 26 |
| 406.69-435.50 | 2.48-7.98 | Kim et al. [33] | 7 |
| 420.45-513.85 | 3.68-90.44 | Daubert et al. [40] | 14 |
| 467.39, 479.39, 488.15 | 20, 30, 40 | Yang et al. [41] | 3 |
| 519.7-738.4 | 98.59-3985 | VonNiederhausern et al. [42] | 9 |

157

158 3. Experimental Work

159 3.1 Materials

160 Information for the chemicals used are provided in **Table 4**. MDEA was used as received
161 from the supplier without further purification. Ultra-pure Millipore water was used in this work
162 to prepare the aqueous amine solutions. Both the amine and the water were degassed
163 independently and they were mixed under vacuum to eliminate presence of air during the
164 experiment. The solutions were prepared gravimetrically in a METTLER PM1200 scale with
165 an accuracy of $1 \cdot 10^{-5}$ kg. The composition uncertainty is the same for each component in a
166 binary mixture as explained in Appendix, and it was found to be $u(w)=0.002$ for 50.1 wt.%
167 MDEA-H₂O and $u(w)=0.003$ for 70 wt.% MDEA-H₂O. The gases used in this work are
168 hydrogen sulfide and methane as a makeup gas.

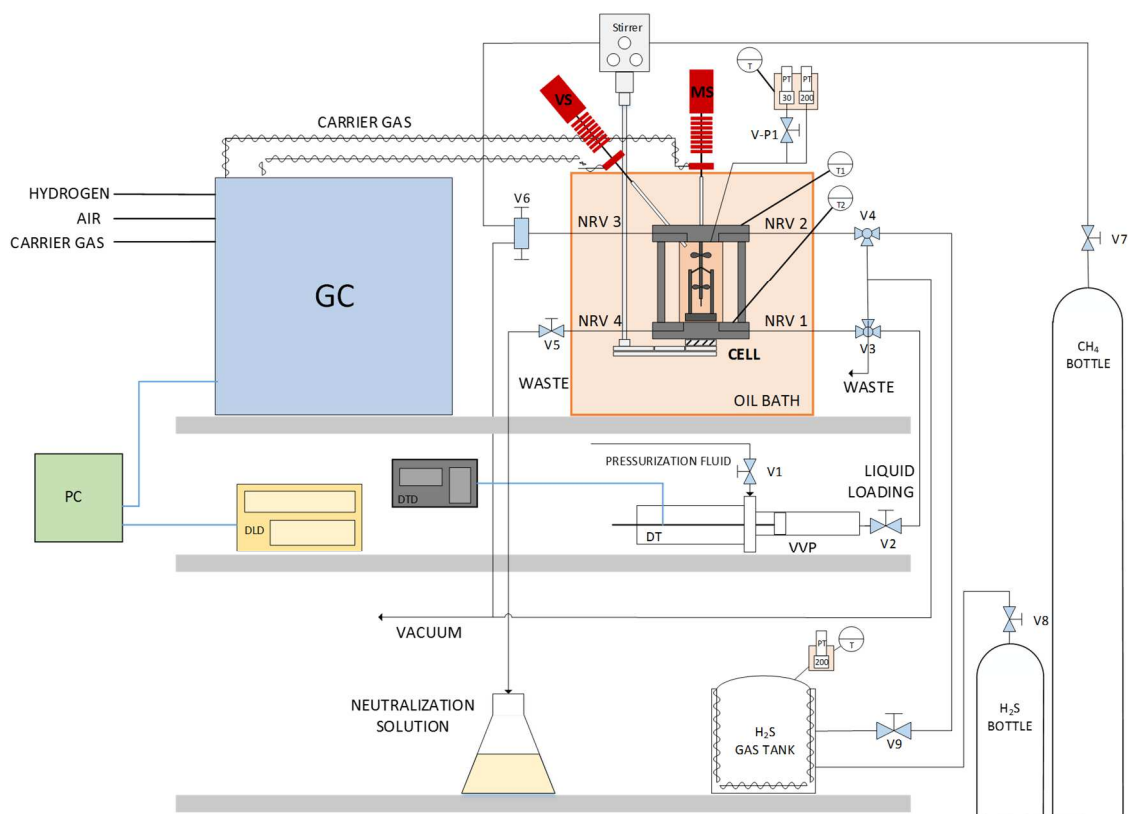
169 **Table 4:** Chemical Sample Table.

| Component | IUPAC name | CAS | Supplier | Purity | Analysis method |
|-------------------------------|---|-----------|---------------|----------------|-----------------|
| N-methyldiethanolamine (MDEA) | 2-[2-hydroxyethyl(methyl)amino] ethanol | 105-59-9 | Sigma-Aldrich | ≥ 99 wt.% | GC |
| Water | Oxidane | - | - | Ultra-pure | - |
| Hydrogen sulfide | Sulfane | 7783-06-4 | Air Liquide | ≥ 99.5 vol.% | GC |
| Methane | Methane | 74-82-8 | Air Liquide | ≥ 99.995 vol.% | GC |

170

171 3.2 Experimental set-ups

172 **High-pressure VLE.** The high-pressure vapor-liquid equilibrium (VLE) experiments were
173 conducted in an in-house manufacture by ARMINES employing the static-analytic method [43]
174 The apparatus is designed for measurements with acid gases and can be operated in the pressure
175 range from 0.5 to 19.9 MPa and temperatures, from 223 to 473 K. Temperature regulation with
176 an accuracy of ± 0.01 K is achieved through immersing the cell into an oil bath. The apparatus
177 is similar to the one previously presented by [29] and its schematic is given in **Figure 1**.



178

179 **Figure 1:** High-pressure VLE setup. DTD: Displacement Transducer Display, DLD: Data Logging
 180 Device, DT: Displacement Transducer, GC: Gas Chromatograph, MS: Mobile Sampler for the analysis
 181 of liquid phase, NRV: Non-Rotating valve, PC: Personal Computer for data acquisition, PT: Pressure
 182 Transducer, T: Thermocouple, V: Valve, VS: Vapor Sampler for the analysis of gas phase, VVP:
 183 variable volume press.

184 The set-up consists of three distinct parts: a) the equipment for filling up the equilibrium
 185 cell, i.e. the variable volume press (VVP), the gas bottles and gas tanks, b) the equilibrium cell,
 186 including automatic samplers for the gas and the liquid phase(s) and c) the equipment for the
 187 analysis of the samples, i.e. the gas chromatograph. Each of these parts consists of various
 188 valves and instrumentation. A variable volume press composed by the variable volume pressure
 189 cell, a piston and a displacement transducer, was used to introduce the liquid inside the cell,
 190 under vacuum. The transducer measures the piston displacement with an accuracy of $\pm 1 \cdot 10^{-5}$
 191 m and, by knowing the exact dimensions of the cell, the exact volume of the solvent introduced
 192 was determined. Approximately $6 \cdot 10^{-6} \text{ m}^3$ of solvent were introduced in every experiment. An
 193 H_2S bottle was connected to a gas tank with volume of $1.61 \cdot 10^{-4} \pm 5 \cdot 10^{-8} \text{ m}^3$, which was further
 194 connected to the cell. The presence of a small gas tank between the gas bottle and the cell was
 195 dictated as an extra safety barrier in case of leakage of the toxic H_2S . Pressurization of the cell
 196 with methane was done directly from the CH_4 bottle.

197 The equilibrium cell is a sapphire tube standing between two Hastelloy flanges. Kalrez O-
198 rings are used for sealing the tube. The upper flange accommodates two non-rotating stem
199 loading valves, for H₂S and for CH₄, and the lower flange accommodates two more, only one
200 of which was used for the loading of the liquid solution and the discharge of the cell. The
201 temperature is monitored and controlled by two platinum probes and two 100 Ω Platinum
202 resistance temperature detectors (Pt100) with an uncertainty of ± 0.02 K. Each of the two
203 located in each flange. They are connected to an HP data acquisition unit and are carefully
204 periodically calibrated. The cell is equipped with two DruckTM pressure transducers, one
205 calibrated for 0–3 MPa and the other for 0-30 MPa pressure range respectively. The transducers
206 are maintained at the temperature they were calibrated at and the uncertainty is 0.6 kPa. The
207 volume of the cell is $33.12 \cdot 10^{-6} \pm 5 \cdot 10^{-8} \text{ m}^3$ (or $32.24 \cdot 10^{-6} \text{ m}^3$ when the low-pressure transducer
208 is isolated). A stirring system is integrated to the cell in order to reduce the time of equilibration
209 and ensure phase homogeneity. The variable-speed stirrer is composed by a rotating axis inside
210 the cell, two propellers mounted on the rotating axis for stirring both the gas phase and the
211 liquid phase and a magnetic rod mounted on the rotating axis in order to allow for rotation of
212 the axis by a stirring motor located below the cell.

213 Agilent software BenchLink is used for online monitoring of pressure and temperature,
214 enabling the determination of equilibrium. Once the equilibrium is reached, micro samples can
215 be withdrawn and transferred to the GC for analysis. Automatic sampling is allowed through
216 two capillary samplers (ROLSI[®]) Armines' patent [44]. Two capillaries are fixed in the
217 cylindrical wall of the cell at levels designed to withdraw vapor and liquid phase samples. The
218 samplers are connected to a PERICHRON model PR-2100 gas chromatograph, through a
219 heated transfer line. The temperature selected is higher than the boiling point of the heaviest
220 component (MDEA) to avoid any sample condensation. The chromatograph is equipped with a
221 thermal conductivity detector (TCD) and a flame ionization detector (FID), and WINILAB III
222 software is used for GC acquisition and treatment.

223 **Ebulliometer.** A modified Swietoslowski ebulliometer was used, described earlier in detail
224 by Kim et al. [33]. The apparatus can be operated at temperatures up to 473 K and at sub-
225 atmospheric and atmospheric pressure. The temperatures were measured with calibrated Pt100
226 resistance thermosensors with an uncertainty of ± 0.05 K. A DP1520 pressure controller from
227 DruckTM was used, calibrated against a BeamexC5 calibrator with an accuracy of ± 0.03 kPa.
228 The solution is accommodated inside a $2 \cdot 10^{-4} \text{ m}^3$ glass equilibrium still and the set-up allows
229 for the sampling of both the vapor and the liquid phase.

230

3.3 Experimental Procedure

231 **High-pressure VLE.** After thorough cleaning with hot deionized (DI) water and ethanol, the
 232 cell and tubings were left to dry and set to vacuum during the previous night. The solution was
 233 prepared under vacuum directly inside the VVP and the solution preparation temperature was
 234 approximately 298 K. Back-pressure of ca. 500 kPa of methane was applied to the VVP. The
 235 solution was introduced inside the cell, and the end displacement position was recorded, so as
 236 the exact amount of solution added could be calculated. The cell was immersed into the bath,
 237 the stirrer was turned on, the temperature of the experiment was set and the system was left to
 238 equilibrate. Temperature stabilization required approximately 30-60 min, after which the vapor
 239 pressure of the solution was recorded.

240 The desired global loading, i.e. mol of H₂S inside the cell per mol of amine, was first decided
 241 and based on the PVT conditions of the H₂S gas tank before and after the filling of the cell, the
 242 amount of H₂S introduced was determined. The calculations were performed using REFPROP
 243 software [45] and a Helmholtz energy-based equation of state developed by [46] for pure H₂S
 244 was used. The global loading was, thus, calculated by:

$$n_{H_2S} = n_{H_2S,tank}^{before} - n_{H_2S,tank}^{after} \quad \text{Eq. 2}$$

$$\alpha_{glob} = \frac{n_{H_2S}}{n_{MDEA}} \quad \text{Eq. 3}$$

245 For the experiments with the 50.1 wt.% MDEA aqueous solution, initially a small amount of
 246 H₂S was introduced and it was left to equilibrate. Reaction of H₂S and MDEA is fast and
 247 equilibrium was reached within one hour. Because the total pressure was lower than the
 248 minimum required pressure of 500 kPa for the ROLSI[®] samplers and GC to function, methane
 249 was added up to 500 kPa. Equilibrium was reached in approximately one hour, and the sampling
 250 started. In our experiments, sampling and analysis was conducted only for the vapor phase.
 251 Higher loadings were reached by adding more H₂S into the cell and repeating the above-
 252 mentioned procedure.

253 For the 70 wt.% MDEA solution VLE investigation, two series of experiments were
 254 conducted based on the global loading, one for 0.2 and one for 0.5 mol H₂S/mol MDEA
 255 approximately. The experimental procedure varies in the way that after equilibrium was
 256 reached, methane was added in 3 stages, up to 2000, 6000 and 10000 kPa. At each pressure
 257 level, sampling and analysis of the vapor phase was performed upon equilibrium. The
 258 experiments were performed under isothermal conditions, at 283, 353 and 393 K. At the end of

259 the experiment, the cell was depressurized and emptied safely through a caustic solution
 260 (NaOH) in order to neutralize the system. At each temperature, a new experiment was
 261 conducted using fresh solution. We aimed at having the same global loading at all temperatures,
 262 however it was not practically possible to reach exactly the same loadings in every experiment.
 263 The study at each temperature and global loading lasted approximately one week.

264 The analysis of vapor phase concentration was performed in a GC equipped with a Porapak-
 265 R column R80/100 mesh (length 2 m, diameter 2 mm) from RESTEK. The carrier gas was
 266 helium at a flow rate of 20 ml/min. A constant temperature program at 363 K was used for the
 267 quantification of both methane and hydrogen sulfide. Analysis at 383 K was also performed to
 268 check for water presence in the vapor phase. In order to check the repeatability of the
 269 measurements and to perform uncertainty analysis, five samples at least were withdrawn, the
 270 first two of them usually were required to saturate the transfer lines in terms of adsorption.
 271 Disturbance to equilibrium was considered negligible due to the small volume of each sample.

272 Knowing the pressure, temperature and the composition of the vapor phase, the density of
 273 the vapor phase was estimated using REFPROP software [45]. The amount of n_{H_2S} in the vapor
 274 and liquid phase and finally the H_2S loading in the liquid phase, liquid loading α , were
 275 calculated according to Eq. 4 - Eq. 7.

$$n_{tot}^v = \rho^v \cdot V^v \quad \text{Eq. 4}$$

$$n_i^v = n_{tot}^v \cdot y_i \quad \text{Eq. 5}$$

$$n_i^l = n_{tot} - n_i^v \quad \text{Eq. 6}$$

$$\alpha = \frac{n_{H_2S}^l}{n_{MDEA}} \quad \text{Eq. 7}$$

276 where ρ^v is the molar density of the gas mixture, calculated using REFPROP and V^v is the
 277 volume of the vapor phase. The latter is the difference between the volume of the cell, ca. $33 \cdot 10^{-6}$
 278 m^3 , which is known from our calibration data and the volume of the liquid which was
 279 estimated by the correlations proposed by [15], assuming that the effect of pressure in the liquid
 280 volume is negligible. Bernal-García and coworkers measured the density of aqueous MDEA in
 281 the whole composition range at temperature range of 263.15 - 363.15 K and, based on their
 282 data, calculated the excess molar volumes of the binary systems. For our calculations at the
 283 temperature of 393 K which was not studied in the afore-mentioned work, the excess molar
 284 volume was extrapolated. It is worth mentioning that the deviations in number of moles of H_2S
 285 calculated by the Ideal Gas Law equation and REFPROP employing the most up-to-date

286 Helmholtz energy-based EoS led to deviations in the liquid loading lower than 1.5% at 283 and
287 353 K, while the deviations were higher at 393 K (max 2.7%). For more accurate results, we
288 used the results based on the latter.

289 **Ebulliometer.** Approximately $0.8 \cdot 10^{-4} \text{ m}^3$ of liquid was charged inside the still, preceding purge
290 with nitrogen. The desired temperature was set and equilibrium was assumed after 10 min of
291 stable pressure and temperature. The vapor pressure of MDEA was measured at the temperature
292 range of 405 – 435 K. Validation of the apparatus was performed by measuring the vapor
293 pressure of water and a 1.5% maximum error from the literature was found in equilibrium
294 pressure.

295 4. Thermodynamic modeling

296 **High pressure VLE.** An in-house MATLAB-based rigorous model has been developed to
297 describe the chemical and phase equilibrium for the system H_2S -MDEA- H_2O . The same
298 algorithm has been previously used to successfully describe CO_2 -amine- H_2O systems relevant
299 to carbon capture processes [47], [48]. Peng-Robinson EoS [49] with the original alpha function
300 was employed to describe the non-idealities of the vapor phase, coupled with the traditional van
301 der Waals one-fluid mixing rules. The binary interaction parameters for Peng-Robinson EoS in
302 this work were set to zero. To account for the non-idealities in the liquid phase, the electrolyte
303 non-random two-liquid (eNRTL) model [50] was utilized. The models are presented in the
304 Appendix. The required critical parameters and acentric factors for pure components are given
305 in Supplementary Information.

306 The chemical reactions assumed in the liquid phase are the ionization of water, the
307 protonation of MDEA and the dissociation of H_2S (R. 1-3). The second dissociation reaction of
308 hydrogen sulfide, from bisulfide to sulfide, is not considered in our model due to the low
309 concentration of S^{2-} in the solution and in order to reduce the number of parameters in the model
310 [16].



311

312 The chemical equilibrium constants as well as Henry's constant for hydrogen sulfide are
 313 described by Eq. 8, parametrized according to **Table 5**, where x stands for either the chemical
 314 equilibrium constant K_{eq} or Henry's constant H_{H_2S} . Temperature is expressed in K and Henry's
 315 constant for hydrogen sulfide in kg·atm.

$$\ln(x) = A + \frac{B}{T} + C \ln(T) + DT \quad \text{Eq. 8}$$

316

317 **Table 5.** Mole fraction-based parameters for Eq. 8, reported only with their significant digits.

| | A | B | C | D | Reference |
|--|---------|--------|----------|---------|----------------------|
| Chemical Equilibrium constant for R. 1 | 132.89 | -13445 | -22.477 | 0 | Posey [36] |
| Chemical Equilibrium constant for R. 2 | -60.03 | -1974 | 7.533 | 0 | Oscarson et al. [51] |
| Chemical Equilibrium constant for R. 3 | 214.58 | -12995 | -33.547 | 0 | Posey [36] |
| Henry's constant for H ₂ S | 342.595 | -13237 | -55.0551 | 0.05957 | Edwards et al. [52] |

318

319 The vapor pressure for hydrogen sulfide and water is estimated using the Riedel correlation
 320 (Eq. 9) where T expressed in K and P^{sat} in Pa. The parameters are presented in **Table 6**. MDEA
 321 vapor pressure has been measured in this work and fitted to Antoine correlation. The Antoine
 322 parameters used in this work can be found in **Section 1.5.2**.

$$\ln(P^{sat}) = A + \frac{B}{T} + C \ln(T) + DT^E \quad \text{Eq. 9}$$

323 **Table 6.** Parameters for pure component vapor pressure correlations for Eq. 9.

| Component | Model | A | B | C | D | E | Reference |
|------------------|--------|--------|-------|---------|---------|-------|------------|
| H ₂ S | Riedel | 106.47 | -5018 | -13.306 | -0.09 | -0.13 | DIPPR [53] |
| H ₂ O | Riedel | 73.649 | -7258 | -7.304 | 4.2E-06 | 2 | DIPPR [53] |

324

325 A sensitivity analysis was performed to evaluate the significant numbers in the parameters
 326 retrieved from the literature. In **Table 5** and **Table 6** the parameters are provided only with their
 327 significant digits.

328 The adjustable parameters for the eNRTL model are the non-randomness factors, α , and the
 329 energy parameters, τ_{ij} . The optimization of the H₂S-MDEA-H₂O system requires the regression
 330 of a total of 78 parameters. In order to reduce this high number of parameters to be adjusted,
 331 the following steps have been taken:

332 I) All non-randomness factors α have been given fixed values according to **Table 7**.
333 II) The energy parameters for the subsystem H₂S-H₂O have been fixed to the default values
334 used in Aspen Plus V10 simulation software (**Table 7**).
335 III) The energy parameters for the subsystem MDEA-H₂O have been fixed to the values
336 obtained by the regression of the literature data presented in **Subsection 2.2 MDEA-H₂O**
337 **system**.
338 As a result, the number of parameters is reduced to 36. The temperature dependency of the
339 energy parameters is described by Eq. 10, where a_{ij} and b_{ij} were fitted to experimental data.

$$\tau_{ij} = a_{ij} + \frac{b_{ij}}{T} \quad \text{Eq. 10}$$

340 The fixed non-randomness factors and fixed energy parameter values are presented in **Table 7**,
341 where m denotes molecule and $c-a$ cation-anion (salt). The non-randomness factors were fixed
342 at 0.2 for molecule-molecule and water-salt interactions, and at 0.1 for the H₂S-salt and MDEA-
343 salt interactions, according to Hessen and coworkers [54].

344

345 **Table 7:** Fixed parameters of eNRTL model used in this work.

| Non-randomness factors, α | | | | | |
|----------------------------------|-----|-----|-----|--|--|
| Components | | | | | |
| i | j | ij | ji | | |
| m | m | 0.2 | 0.2 | | |
| H ₂ O | c-a | 0.2 | 0.2 | | |
| H ₂ S | c-a | 0.1 | 0.1 | | |
| MDEA | c-a | 0.1 | 0.1 | | |

| Energy parameters, τ_{ij} | | | | | |
|--------------------------------|--|----|----|----|----|
| Components | | a | | b | |
| i | j | ij | ji | ij | ji |
| H ₂ O | H ₂ S | 0 | 0 | 0 | 0 |
| H ₂ O | H ₃ O ⁺ -OH ⁻ | 8 | -4 | 0 | 0 |
| H ₂ O | H ₃ O ⁺ -HS ⁻ | 8 | -4 | 0 | 0 |

| | | | | | |
|------------------|--|----|----|---|---|
| H ₂ S | H ₃ O ⁺ -OH ⁻ | 15 | -8 | 0 | 0 |
| H ₂ S | H ₃ O ⁺ -HS ⁻ | 15 | -8 | 0 | 0 |

346

347 The optimization routine used in this work is Particle Swarm Optimization (PSO), developed
 348 by Kennedy and Eberhart [55]. This algorithm allows for the optimization of continuous non-
 349 linear functions, using particle swarm methodology. The advantage of this optimization routine
 350 is that it uses random initialization, thus, unlike other optimization methods, its convergence is
 351 not dependent on the first approximations. In order to avoid local minima and find an optimal
 352 solution, local best topology was used [56], [57]. The PSO parameters are swarm size of 40,
 353 maximum number of iterations 600 in 3 loops which terminate once the optimized value
 354 deviates more than 10^{-4} (tolerance criterion) from its preceding one or if less than 1%
 355 improvement is achieved during 60 iterations. The minimization of the absolute average relative
 356 deviation (AARD) shown in Eq. 11, was chosen as the objective function, where Y was either
 357 the partial pressure of H₂S, P_{H_2S} , or the total pressure, P_{tot} .

$$F_{obj}(\%) = \frac{1}{N} \sum_i^N \frac{|Y_i^{exp} - Y_i^{pred}|}{Y_i^{exp}} \cdot 100 \quad \text{Eq. 11}$$

358 5. Results and Discussion

359 5.1 Experimental results

360 **High-pressure VLE.** The experimental vapor-liquid equilibrium data obtained in this work
 361 with 50.1 wt.% and 70 wt.% MDEA solution for the system CH₄-H₂S-MDEA-H₂O at various
 362 pressures and temperatures are presented in **Table 8** and **Table 9**. As mentioned earlier,
 363 knowing the experimental uncertainty of reported data could possibly help us understand the
 364 scatter observed in the data for the system H₂S-MDEA-H₂O. Therefore, we performed a
 365 thorough investigation of our measurements' uncertainty in order to properly evaluate our data
 366 and conclude on the impact of experimental uncertainty on our results.

367 We have reported the combined uncertainties employing the Law of propagation of
 368 uncertainty according to NIST guidelines [58]. The new data are accompanied by the standard
 369 uncertainties for total pressure and temperature as well as the combined uncertainties for the

370 partial pressure of hydrogen sulfide, the global and the liquid loading. It was found that the
 371 main contributor to the uncertainty of the partial pressure of H₂S is the total pressure of the
 372 system, as can be observed by the increasing uncertainty of $P_{\text{H}_2\text{S}}$ for increasing total pressure.
 373 The main contribution to the global loading uncertainty is associated with the loading itself,
 374 while the uncertainty of the liquid loading is mostly affected by the uncertainty of the total
 375 moles of H₂S introduced in the cell. The repeatability of our measurements was taken into
 376 account by virtue of the multiple samples analyzed on the GC at each equilibrium pressure and
 377 temperature. The complete uncertainty analysis can be found in Supporting Information.

378

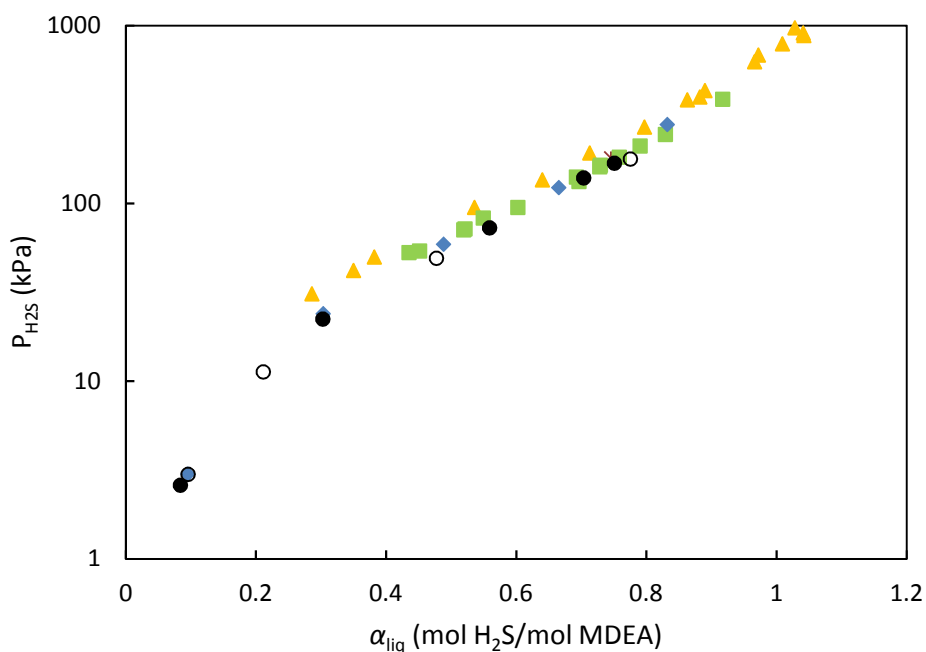
379 **Table 8.** Experimental vapor-liquid equilibrium data and their corresponding combined
 380 uncertainties at total pressure of 500 kPa (and one measurement at total pressure 3000 kPa) and
 381 temperature of 323 K for the system CH₄-H₂S-MDEA-H₂O and 50.1 wt.% aqueous MDEA.
 382 Methane is used as makeup gas.

| T | P_{tot} | $P_{\text{H}_2\text{S}}$ | $u_c(P_{\text{H}_2\text{S}})$ | α_{glob} | $u_c(\alpha_{\text{glob}})$ | α_{liq} | $u_c(\alpha_{\text{liq}})$ | NS |
|--------------|------------------|--------------------------|-------------------------------|---|---|---|---|----|
| K | kPa | kPa | kPa | mol H ₂ S global/ mol MDEA | mol H ₂ S global/ mol MDEA | mol H ₂ S liquid/ mol MDEA | mol H ₂ S liquid/ mol MDEA | |
| Experiment 1 | | | | | | | | |
| 322.98 | 493.81 | 2.99 | 0.03 | 0.096 | 0.003 | 0.095 | 0.001 | 9 |
| 322.98 | 480.01 | 11.27 | 0.12 | 0.214 | 0.005 | 0.211 | 0.002 | 9 |
| 322.98 | 500.72 | 49.11 | 0.43 | 0.490 | 0.005 | 0.477 | 0.002 | 7 |
| 322.98 | 604.01 | 177.59 | 1.20 | 0.822 | 0.006 | 0.775 | 0.003 | 10 |
| Experiment 2 | | | | | | | | |
| 322.98 | 493.92 | 2.60 | 0.02 | 0.085 | 0.003 | 0.084 | 0.002 | 6 |
| 322.98 | 493.50 | 22.33 | 0.19 | 0.312 | 0.004 | 0.303 | 0.002 | 6 |
| 322.98 | 498.13 | 72.79 | 0.56 | 0.588 | 0.006 | 0.559 | 0.003 | 8 |
| 322.98 | 530.82 | 139.10 | 0.93 | 0.760 | 0.013 | 0.703 | 0.006 | 5 |
| 322.98 | 545.53 | 168.46 | 1.06 | 0.820 | 0.039 | 0.751 | 0.020 | 9 |
| 322.98 | 3106.96 | 179.67 | 1.52 | 0.820 | 0.039 | 0.745 | 0.020 | 8 |

383 ^aStandard uncertainties not included above are $u(T) = 0.02$ K, $u(P) = 0.6$ kPa.

384 **Table 8** and **Figure 2** reveal information regarding both the reproducibility of the
 385 measurements in this work as well as their comparison with the literature for the system CH₄-
 386 H₂S-MDEA-H₂O with a 50-50.1 wt.% MDEA solution at approximately 323 K. The measured
 387 vapor fractions of methane and hydrogen sulfide are reported in Supporting Information
 388 together with the uncertainty analysis. Our measurements in the presence of 500 kPa of methane

389 were performed in two different experiments, and as one can observe in the figure, the same
 390 behavior is followed and the measurements can be reproduced. The data obtained in this work
 391 are in agreement with the data reported by Dicko et al. [29] under similar conditions. These
 392 data together with Sadegh et al.'s data [30] at total pressure of 1500 kPa and 7000 kPa show
 393 that, for a given liquid loading, an increase in the total pressure of the system leads to an increase
 394 in the H₂S partial pressure. Our single measurement at total pressure of 3000 kPa for this system
 395 follows this trend, too. An exception is the last point reported by Dicko et al. at $\alpha_{liq} = 0.832$ mol
 396 H₂S / mol MDEA, which also differs from the trend in our data. This point is measured at total
 397 pressure 700 kPa but lies between the data reported by Sadegh et al. at 1500 kPa and 7000 kPa
 398 total pressure. Here it is important to mention that the measurements reported by Dicko et al.
 399 are global loadings, and the liquid loadings shown in **Figure 2** are the ones calculated by the
 400 authors.



401
 402 **Figure 2:** Equilibrium H₂S partial pressures as a function of liquid loading and total pressure
 403 for 50 wt.% MDEA-H₂O at 323 K. ● $P_{tot} = 500$ kPa (This work, Experiment 1), ○ $P_{tot} = 500$ -
 404 600 kPa (This work, Experiment 2), ◆ $P_{tot} = 500$ -700 kPa [29], ■ $P_{tot} = 1500$ kPa [30], × $P_{tot} =$
 405 3000 kPa (This work), ▲ $P_{tot} = 7000$ kPa [30].

406
 407 **Table 9.** Experimental vapor-liquid equilibrium data and their corresponding combined
 408 uncertainties as a function of total pressure and temperature for the system CH₄-H₂S-MDEA-
 409 H₂O and 70 wt.% aqueous MDEA^a. Methane is used as makeup gas.

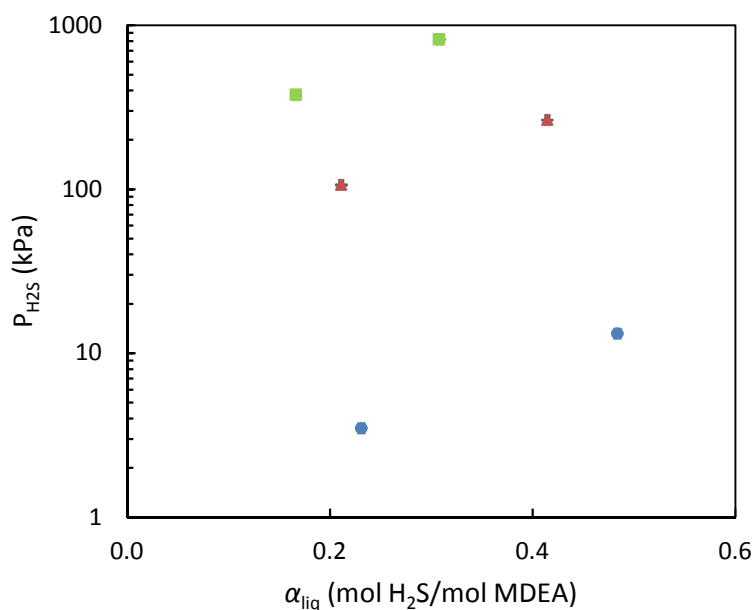
| T | P_{tot} | $P_{\text{H}_2\text{S}}$ | $u_c(P_{\text{H}_2\text{S}})$ | α_{glob} | $u_c(\alpha_{\text{glob}})$ | α_{liq} | $u_c(\alpha_{\text{liq}})$ | NS |
|--------|------------------|--------------------------|-------------------------------|--|--|--|--|----|
| K | kPa | kPa | kPa | mol H ₂ S global/ mol MDEA | mol H ₂ S global/ mol MDEA | mol H ₂ S liquid/ mol MDEA | mol H ₂ S liquid/ mol MDEA | |
| 283.00 | 2011.87 | 3.48 | 0.03 | 0.232 | 0.003 | 0.231 | 0.003 | 9 |
| 283.00 | 6030.85 | 3.85 | 0.05 | 0.232 | 0.003 | 0.231 | 0.003 | 10 |
| 283.00 | 10052.50 | 4.68 | 0.04 | 0.232 | 0.003 | 0.231 | 0.003 | 7 |
| 352.99 | 1976.07 | 106.23 | 0.92 | 0.239 | 0.002 | 0.211 | 0.002 | 5 |
| 352.99 | 3954.66 | 108.30 | 0.98 | 0.239 | 0.002 | 0.210 | 0.002 | 10 |
| 352.99 | 5957.76 | 108.03 | 1.03 | 0.239 | 0.002 | 0.210 | 0.002 | 7 |
| 352.99 | 7976.36 | 111.95 | 1.04 | 0.239 | 0.002 | 0.209 | 0.002 | 6 |
| 352.99 | 9988.18 | 111.42 | 1.12 | 0.239 | 0.002 | 0.208 | 0.002 | 6 |
| 393.00 | 2024.40 | 375.10 | 1.46 | 0.246 | 0.002 | 0.167 | 0.002 | 8 |
| 392.99 | 5979.36 | 376.17 | 1.72 | 0.246 | 0.002 | 0.165 | 0.002 | 10 |
| 393.00 | 9925.29 | 364.18 | 1.97 | 0.246 | 0.002 | 0.167 | 0.002 | 8 |
| 283.00 | 1975.74 | 13.13 | 0.15 | 0.488 | 0.002 | 0.484 | 0.002 | 7 |
| 283.00 | 5990.55 | 17.37 | 0.28 | 0.488 | 0.002 | 0.482 | 0.002 | 5 |
| 283.00 | 10045.17 | 21.56 | 0.24 | 0.488 | 0.002 | 0.480 | 0.002 | 6 |
| 352.92 | 2006.00 | 264.36 | 1.30 | 0.478 | 0.002 | 0.415 | 0.002 | 7 |
| 352.92 | 5980.37 | 281.97 | 1.57 | 0.478 | 0.002 | 0.408 | 0.002 | 8 |
| 352.92 | 9975.23 | 300.30 | 1.67 | 0.478 | 0.002 | 0.402 | 0.002 | 8 |
| 393.05 | 974.22 | 834.43 | 0.49 | 0.484 | 0.002 | 0.304 | 0.003 | 3 |
| 393.00 | 2034.17 | 818.12 | 2.26 | 0.484 | 0.002 | 0.308 | 0.003 | 8 |
| 393.01 | 5893.45 | 806.74 | 3.34 | 0.484 | 0.002 | 0.309 | 0.003 | 7 |
| 393.00 | 9915.85 | 809.32 | 3.68 | 0.484 | 0.002 | 0.307 | 0.003 | 9 |

410 ^a Standard uncertainties not included above are $u(T) = 0.02$ K, $u(P) = 0.6$ kPa.

411 The observation of increased H₂S partial pressure upon increase in total pressure can be
412 made also for the 70 wt.% aqueous MDEA system for the temperatures of 283 K and 353 K.
413 The deviations in partial pressure are higher for higher global loadings. On the other hand, the
414 liquid loading remains unchanged at 283 K while the one at 353 K seems to decrease. At 393
415 K, not clear trends are shown. This behavior is noticed for all global loadings, though the fact
416 that the water present in the vapor phase could not be quantified through the GC analysis, and
417 it was therefore calculated based on the vapor pressure of the solvent under the assumption that

418 it was constant with increasing total pressures, might have its share on the latter. The effect of
419 temperature is the expected one given the exothermic nature of the chemical reactions; the lower
420 the temperature, the higher the absorption of H₂S in the liquid phase at constant partial pressure
421 of hydrogen sulfide. The features discussed above are illustrated in **Figure 3** and **Figure 4**. It
422 is worth mentioning that error bars representing the uncertainty in pressures and loadings are
423 included in the figures, however uncertainties in pressure are too low to be visible.

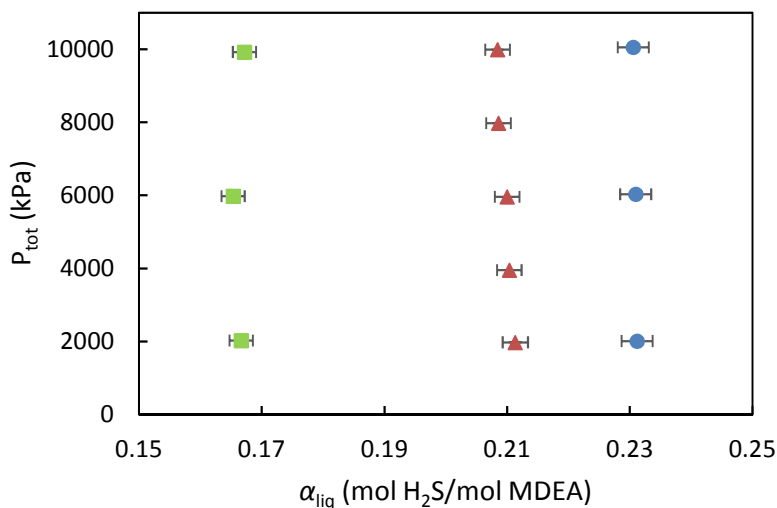
424



425

426 **Figure 3:** Experimental H₂S solubility in a 70 wt.% MDEA-H₂O system with methane as
427 makeup gas at total pressure of 2000 kPa at temperature; ● 283 K, ▲ 353 K and ■ 393 K. Error
428 bars for both H₂S partial pressure and loading are included.

429



430

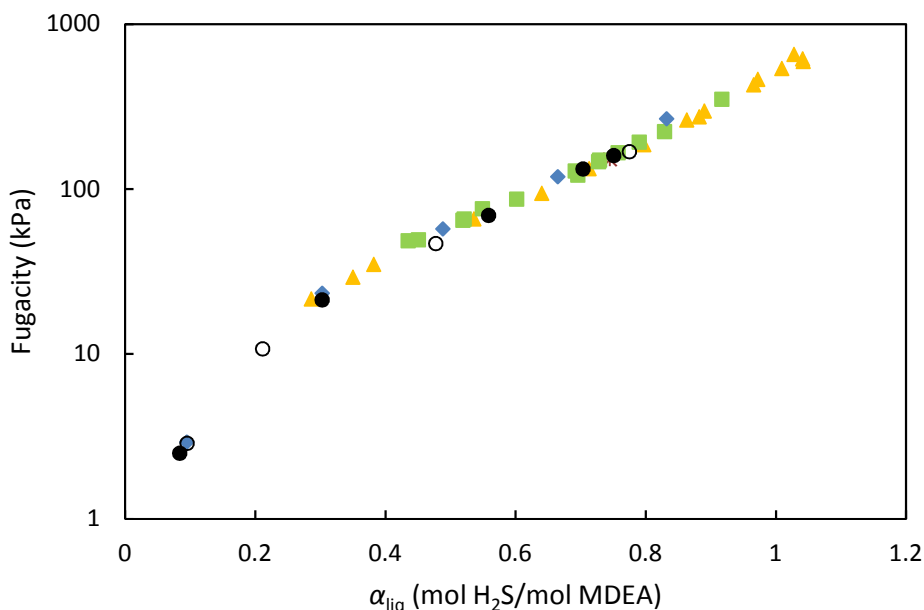
431 **Figure 4:** H₂S liquid phase loading of a 70 wt.% MDEA-H₂O system with methane as makeup
 432 gas as a function of total pressure and temperature; ● 283 K, ▲ 353 K and ■ 393 K. Error bars
 433 for both total pressure and liquid loading are included.

434

435 Although there is a clear trend of the pressure effect on the partial pressure of H₂S, taking
 436 into account the uncertainties, it can be seen that the deviations in liquid loading are similar to
 437 the experimental uncertainty. In fact, at 283 K and for global loading 0.232, no change at all in
 438 liquid loading is observed. The fact that hydrogen sulfide is chemically bound to the amine
 439 reinforces the argument that the differences in loading are due to uncertainty in measurements.
 440 The amount of methane dissolved in the liquid phase is too low to have an impact on the reaction
 441 of hydrogen sulfide with the amine solution which is an exothermic reaction whose reversion
 442 requires high amounts of energy. Overall, it is observed that the effect of increasing the total
 443 pressure from 2000 kPa to 10000 kPa in terms of H₂S loading in a 70 wt.% aqueous MDEA at
 444 temperatures of 283 K, 353 K and 393 K is not significant and, in most cases, it is within or
 445 very close to experimental uncertainty.

446 As Sadegh et al. [30] showed, taking into account the gas fugacities is adequate to explain
 447 the deviations of the equilibrium H₂S pressures at different total pressures for a 50 wt.%
 448 aqueous MDEA. Indeed, **Figure 5** shows how the fugacity exhibits the same behavior for all
 449 data obtained in a 50-50.1 wt.% MDEA-H₂O solution in the presence of methane from different
 450 literature sources. The figure is similar to one provided by Sadegh et al. [30], this time enriched
 451 with our data at total pressure of 500 and 3000 kPa demonstrating the same behavior. The
 452 fugacities were calculated using Peng-Robinson EoS with binary interaction parameters set to
 453 zero. As far as the data obtained for the 70 wt.% aqueous MDEA are concerned, the fugacity

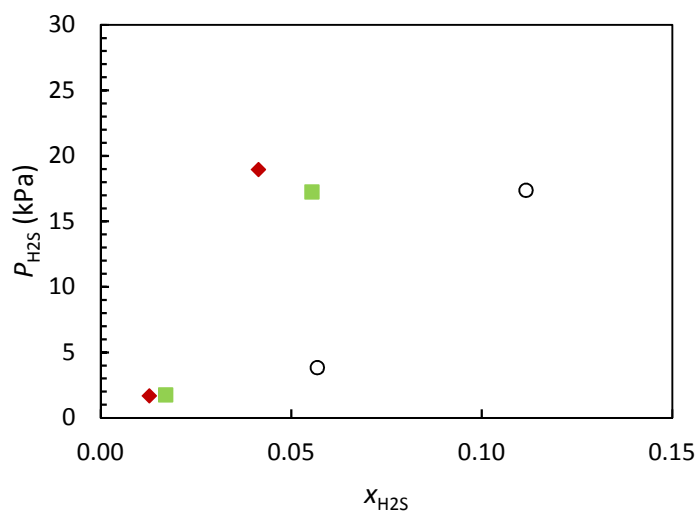
454 can explain the partial pressure trend observed for our data at 283 K and 353 K. At 393 K, the
 455 uncertainty in liquid loadings are such that no solid conclusions can be drawn.



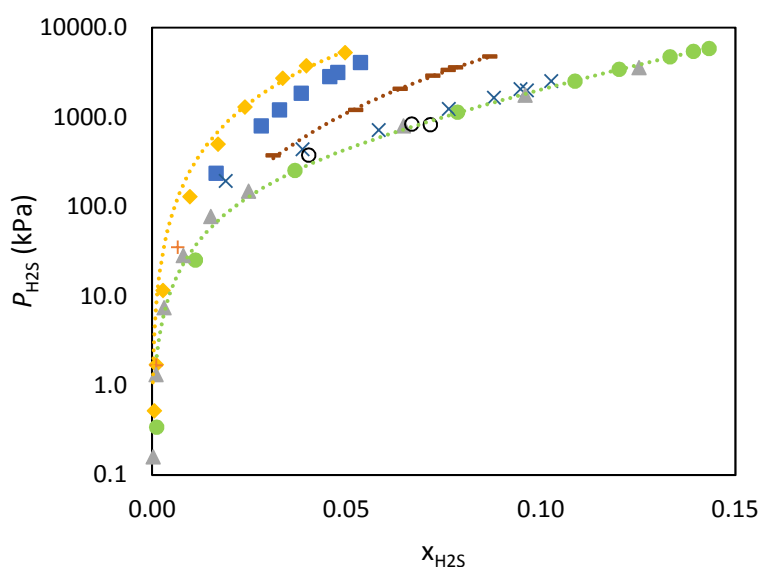
456
 457 **Figure 5:** Equilibrium H₂S fugacities as a function of liquid loading and total pressure for 50
 458 wt.% MDEA-H₂O at 323 K. ● $P_{\text{tot}} = 500$ kPa (This work, Experiment 1), ○ $P_{\text{tot}} = 500\text{-}600$ kPa
 459 (This work, Experiment 2), ◆ $P_{\text{tot}} = 500\text{-}700$ kPa [29], ■ $P_{\text{tot}} = 1500$ kPa [30], × $P_{\text{tot}} = 3000$ kPa
 460 (This work, Experiment 2), ▲ $P_{\text{tot}} = 7000$ kPa [30].

461
 462 The effect of amine concentration was also studied by means of comparison with reported
 463 data in the literature at 283 K and 393 K, shown in **Figure 6** and **Figure 7** respectively. Data at
 464 353 K in our range of loading and pressure are not available in the literature, therefore no
 465 comparison could be performed. A clear effect of increasing molar concentration with
 466 increasing amine concentration and constant H₂S pressure can be seen in the comparison
 467 performed at 283 K. This can be expected since the more amine available, the higher the
 468 capacity of the solvent. It is important to state that the literature data are reported only from one
 469 reference source [25] where methane makeup gas was also used. Because of the effect of
 470 methane presence, we have plotted the available data at similar total pressures; our data only
 471 for total pressure of 6000 kPa and the literature data at total pressure of 6900 kPa in order to
 472 allow for a fairer comparison. The molar concentration of H₂S is also increasing with amine
 473 content in the solution at 393 K, but only up to 50 wt.%. Our data at 70 wt.% overlap with the
 474 literature data obtained in a 50 wt.% aqueous MDEA study. This is illustrated in **Figure 7** where

475 we have only plotted the data with very little methane or with total pressure of 2000 kPa from
476 our work.



477
478 **Figure 6:** Hydrogen sulfide molar concentration in the liquid phase for the system CH₄-H₂S-
479 MDEA-H₂O as a function of partial pressure and amine concentration at total pressures 6000-
480 6900 kPa and at 283 K; ♦ 35 wt.% MDEA-H₂O [25], ■ 50 wt.% MDEA-H₂O [25], ○ 70 wt.%
481 MDEA-H₂O (This work).



482
483 **Figure 7:** Hydrogen sulfide molar concentration in the liquid phase for the system H₂S-MDEA-
484 H₂O as a function of partial pressure and amine concentration at 393 K; ♦ 11.8 wt.% MDEA-
485 H₂O [12], ■ 18.7 wt.% MDEA-H₂O [17], + 23.1 wt.% MDEA-H₂O [23], - 32.2 wt.% MDEA-

486 H₂O [17], ● 48.8 wt.% MDEA-H₂O [12], × 48.8 wt.% MDEA-H₂O, ▲ 50 wt.% MDEA-H₂O
487 [23], ○ 70 wt.% MDEA-H₂O (This work).

488

489 Hydrogen sulfide can react directly with MDEA through a typical acid-base reaction [2]. At
490 the same time, the presence of water would enhance the acid gas uptake through the dissolution
491 of hydrogen sulfide as well the protonation of the amine. Therefore, we could identify two
492 possible mechanisms through which H₂S is absorbed; one directly into the amine and one via
493 water. Moreover, hydrogen sulfide absorption in MDEA-H₂O is the result of both physical and
494 chemical absorption. Therefore, in order to provide a good discussion about the behavior
495 observed in **Figure 6** and **Figure 7**, the physical absorption of hydrogen sulfide into MDEA-
496 H₂O systems should be taken into account. To our best knowledge, only Rinker and Sandall
497 [59] have reported such information. They measured H₂S solubility in protonated aqueous
498 MDEA and their measurements showed that the solubility increases with amine content.
499 Although the available data cover 0-50 wt.% MDEA-H₂O systems, it can be assumed that the
500 same trends would be followed and the physical absorption of H₂S in to a 70 wt.% aqueous
501 MDEA is higher than in a 50 wt.% aqueous MDEA.

502 Based on the above, the fact that $x_{\text{H}_2\text{S}}$ is not increased with amine content from 50 to 70 wt.%
503 at 393 K and constant H₂S pressure indicates that the contribution of the chemical absorption
504 decreases as the amine content increases. This can be also confirmed by observing the slope of
505 indicative tendency curves in **Figure 7** (better illustrated in Figure S7 in Supporting
506 Information, where non-logarithmic scale is used for the y axis). The slope reveals information
507 about the absorption capacity of the systems. It is observed that as the amine composition
508 increases, the P - x curve has a lower slope (apparent Henry's constant). The lower the slope, the
509 closer to linearity and, thus, higher physical absorption. For example, at 500 kPa, the apparent
510 Henry's constant is 535 kPa·m³/kmol for 11.8 wt.% MDEA-H₂O and 300 kPa·m³/kmol for 48.8
511 wt.% MDEA-H₂O at 393 K. This behavior is followed also at higher pressure; at 3000 kPa, the
512 apparent Henry's constant is 1169 kPa·m³/kmol for 11.8 wt.% MDEA-H₂O and 715
513 kPa·m³/kmol for 48.8 wt.% MDEA-H₂O at 393 K. Unfortunately, our data are too few to assess
514 the P - x linearity for 70 wt.% MDEA-H₂O, nonetheless it can be said that the chemical
515 contribution in the overall H₂S uptake is decreased. In the case of low temperatures such as in
516 our studied temperature of 283 K, these effects could probably not be visible because the
517 absorption capacity is very high and our data as well as the data reported in the literature are
518 produced for low H₂S partial pressure.

519

520 **Ebulliometer.** The measurements conducted in the ebulliometer are shown in **Table 10**. The
 521 main limitation of ebulliometric measurements is the absence of stirring. Experimental
 522 measurement of the vapor pressure of the binary mixtures used in this work was not possible
 523 because two phases formed, associated with the high viscosity of pure MDEA, i.e. ca. 77 mPa·s
 524 at 298.15 K [60]–[62]. Therefore, only the vapor pressure of MDEA was measured.

525

526 **Table 10.** Experimental vapor pressure P^s / kPa for pure MDEA^a.

| T (K) | P^s (kPa) | | | | |
|---------|--------------|-----------|----------------------|----------------------|----------------------|
| | DIPPR | | | This work (Table 11) | |
| | Experimental | Predicted | ARD (%) ^b | Predicted | ARD (%) ^b |
| 405.34 | 1.79 | 1.95 | 9% | 1.79 | 0% |
| 411.00 | 2.29 | 2.53 | 10% | 2.34 | 2% |
| 415.31 | 2.79 | 3.06 | 10% | 2.86 | 2% |
| 418.58 | 3.29 | 3.54 | 7% | 3.31 | 1% |
| 421.73 | 3.79 | 4.05 | 7% | 3.80 | 0% |
| 424.52 | 4.29 | 4.55 | 6% | 4.28 | 0% |
| 427.21 | 4.79 | 5.09 | 6% | 4.80 | 0% |
| 429.49 | 5.29 | 5.59 | 6% | 5.28 | 0% |
| 431.60 | 5.79 | 6.08 | 5% | 5.76 | 0% |
| 433.49 | 6.29 | 6.56 | 4% | 6.22 | 1% |
| 435.34 | 6.79 | 7.05 | 4% | 6.71 | 1% |

527

^a Standard uncertainties are $u(T)=0.1$ K, $u(P)=0.1$ kPa.

528

$${}^b\text{ARD} (\%) = \frac{|P_s^{\text{pred}} - P_s^{\text{exp}}|}{P_s^{\text{exp}}} \cdot 100$$

529 5.2 Modeling results

530 In this section, we present first the results from the ebulliometer following by the modeling
 531 results for the high-pressure VLE data, since the first ones are used in the model parametrization
 532 for the H₂S-MDEA-H₂O equilibrium.

533
 534 **Ebulliometer.** The Antoine correlation was fitted to available data from the literature (**Table**
 535 **3**) as well as the newly obtained data of this work, covering a large range of temperatures and
 536 pressures. In **Table 10**, our experimental measurements are compared with the predicted vapor
 537 pressures by our fitted Antoine correlation and the DIPPR equation. At the temperature range
 538 of 405-435 K studied in this work, the absolute relative deviation (ARD) between the
 539 experimental and the estimated value is 7% with DIPPR equation and 1% in our correlation,
 540 which has been fitted to available data in the literature covering temperatures from 293 K to
 541 738 K. The new parameters for Antoine correlation proposed for the estimation of the vapor
 542 pressure of MDEA, are shown in **Table 11**. The Average Absolute Relative Deviation (AARD)
 543 is 4% for our correlation and 30% for DIPPR. The high deviation for DIPPR equation is mainly
 544 due to the vapor pressure predictions at temperatures higher than 530 K, which explains the
 545 high AARD. In the fitting, we excluded the data from Kim et al. [33] which are slightly higher
 546 than the data obtained on the same conditions by Daubert et al. [40] as well as our
 547 measurements. However, including those data leads to modeled vapor pressures with only the
 548 slightly higher AARD of 5%.

549

550 **Table 11.** Parameters for the Antoine correlation^a for pure MDEA vapor pressure.

| | A | B | C |
|------|---------------|---------------|---------------|
| MDEA | 9.676 ± 0.014 | -1965.6 ± 8.9 | -99.33 ± 0.69 |

551 ^a $\log_{10} P^S = A + \frac{B}{T+C}$. T in K. P in Pa. Temperature range: 294 – 738 K

552 **High-pressure VLE.** The parameter fitting for the MDEA-H₂O system returned satisfactory
 553 AARDs for all three variables fitted, i.e. VLE (P_{tot}), FPD and H^E , as described in **Sections 2.2**
 554 and **4**. The calculated AARDs for each variable are shown in **Table 12**.

555

556 **Table 12:** AARDs for the fitted P_{tot} , FPD and H^E for the MDEA-H₂O system.

| Variable | Source | AARD (%) |
|------------------|-----------------|----------|
| P_{tot} | Kim et al. [33] | 1.1 |

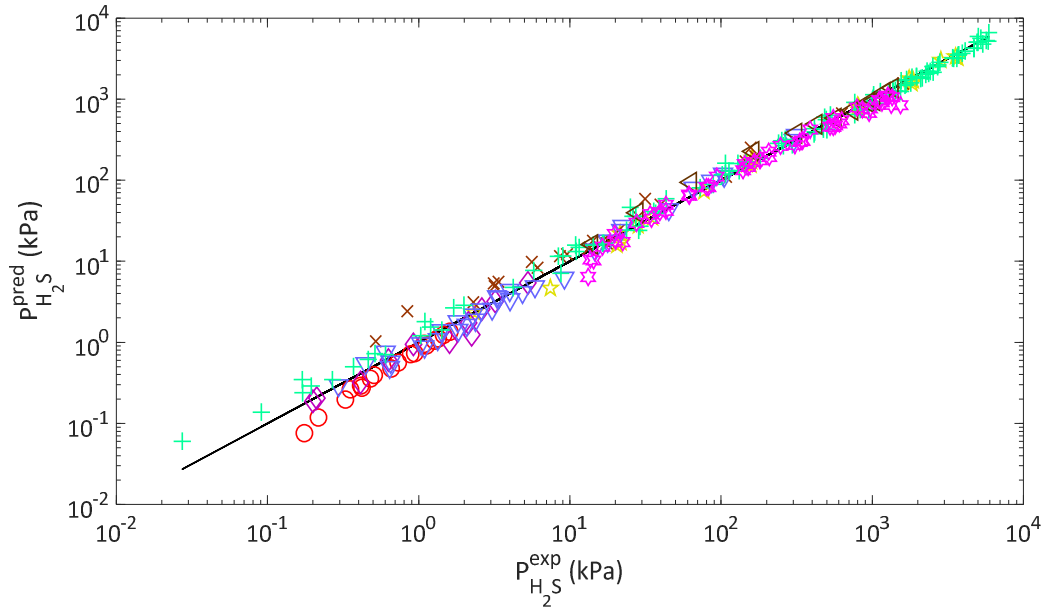
| | | |
|-------|---------------------|------------|
| | Xu et al. [34] | 1.9 |
| | Voutsas et al. [35] | 6.4 |
| | Overall | 2.5 |
| FPD | Chang et al. [31] | 10.3 |
| | Fosbøl et al. [32] | 4.4 |
| | Overall | 6.0 |
| H^E | Posey [36] | 7.6 |
| | Maham et al. [37] | 3.1 |
| | Maham et al. [38] | 11.5 |
| | Overall | 7.4 |

557

558 The model can predict very well the total pressure of the binary system, as witnessed above
559 by the low AARD. The excess enthalpy H^E can be well predicted at temperatures of 298.15 and
560 313.15 K, though the model yields lower excess enthalpies at 338.15 K for MDEA
561 concentrations lower than 85 wt.%. At this temperature, the model was fitted to experimental
562 data reported by Maham et al. [38] which shows the highest AARD. The corresponding figures
563 for the total pressure, excess enthalpy and the freezing point depression are presented in
564 Supporting Information.

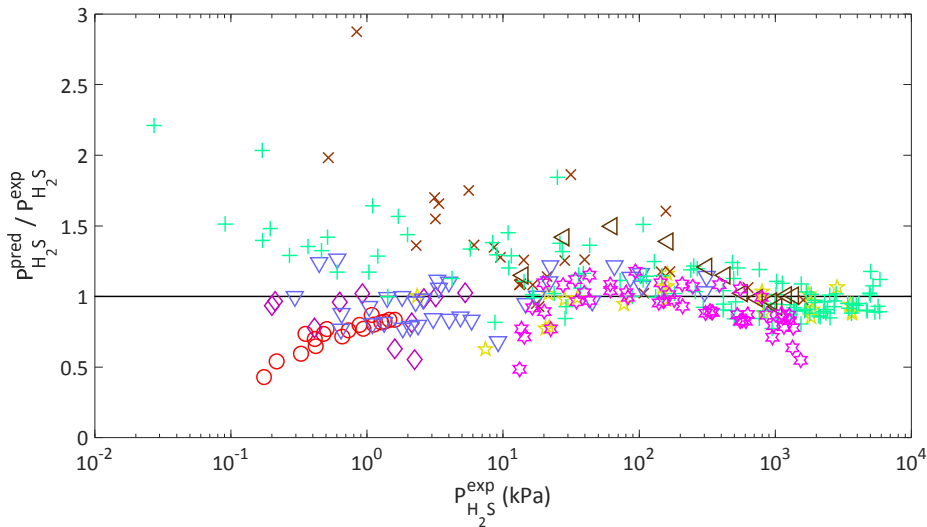
565 The fixed parameters in **Table 7** and the regressed parameters for the binary subsystem
566 MDEA-H₂O (Supplementary Information) were used for the regression of the ternary system
567 H₂S-MDEA-H₂O. Initially, all the data from **Table 1** were used for the parametrization of the
568 model, except for the data from Li and Shen, as well as the data in the presence of methane
569 (Case A). The data obtained in the presence of nitrogen were all included. The scatter already
570 discussed earlier at low loadings resulted in high AARD, especially for the data points reported
571 in terms of partial pressure of H₂S. The high deviations are also attributed to the much lower
572 values of partial pressures in comparison with total ones, leading to higher relative numbers.
573 Therefore, we have decided to also perform the data regression excluding all data at loadings
574 lower than 0.05 mol H₂S/mol MDEA (Case B). This indeed improved substantially the fitting
575 of the partial pressures, as one can see in the AARDs in **Table 13**, from approximately 30% to
576 18%. The parity plot for the predicted and experimental values is shown in **Figure 8** while
577 **Figure 9** shows the difference between predicted and experimental H₂S partial pressure as a
578 function of the experimental value.

579



580

581 **Figure 8:** Parity plot for different literature sources; \circ Lemoine et al. [28], \square Huang and Ng
 582 [23], \diamond Rogers et al. [24], \times (MacGregor and Mather [14], ∇ Jou et al. [21], $+$ Jou et al. [12],
 583 \square Zoghi and Shokouhi [22], \square Maddox et al. [27], $(-)$ $y=x$.



584

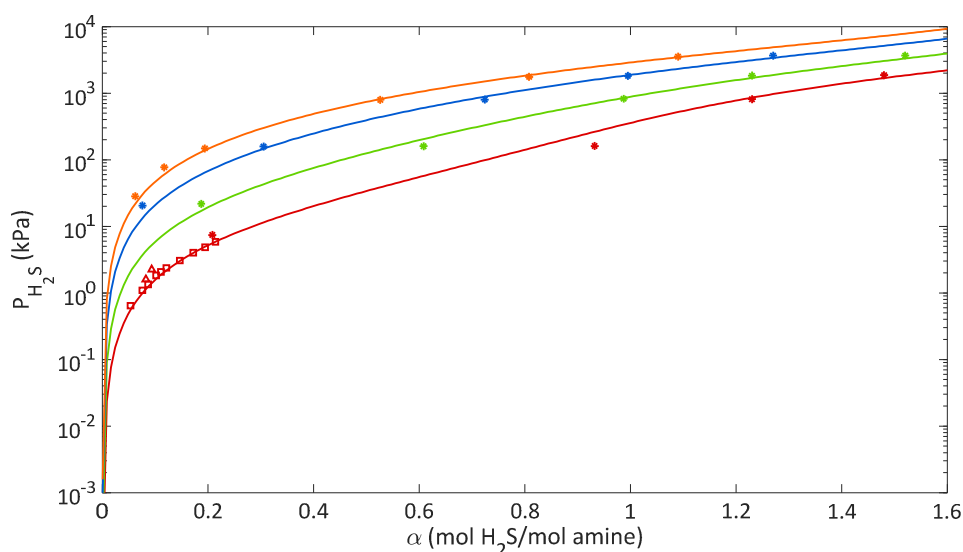
585 **Figure 9:** Difference between predicted and experimental H_2S partial pressure as a function of
 586 the experimental value. \circ Lemoine et al. [28], \square Huang and Ng [23], \diamond Rogers et al. [24], \times
 587 MacGregor and Mather [14], ∇ Jou et al. [21], $+$ Jou et al. [12], \square Zoghi and Shokouhi [22], \square
 588 Maddox et al. [27].

589

590 Significant scatter can be seen in the plots above at the lower pressures. At pressures $P < 1$
 591 kPa, the model underestimates the data from Lemoine et al. [28] while overestimating the data
 592 from Jou et al. [12] and MacGregor and Mather [14]. The accuracy of the model is good for the
 593 data from Rogers et al. [24] and Jou et al. [21], with some data being underpredicted. The visual

594 observations are depicted on the bias and AARD (%) calculations presented in **Table 13**. The
 595 negative bias whose absolute value is the same as the AARD for Lemoine et al.'s work shows
 596 that all data have been underestimated by the model. In addition, the fact that the AAD for this
 597 source is 0.2 kPa shows that the high AARD of 27% is due to the low values in partial pressures.
 598 At intermediate pressures, the scatter is less pronounced, but still the model overpredicts the
 599 data of MacGregor and Mather [14] and Jou et al. [12]. The BIAS and AARDs for these two
 600 are -37% and 38% and -27% and 27% respectively, while the rest of the sources show AARDs
 601 lower than 17%. At higher pressures, both **Figure 8** and **Figure 9** show that the model can
 602 predict well the literature data.

603 Overall, maximum AARD was found for the data from MacGregor and Mather [14] showing
 604 an almost 50% AARD in Case A and 38% in Case B. The minimum deviations observed were
 605 for the data from Maddox et al. [27] in Case A (13%) and from Huang and Ng [23] in Case B
 606 (9%). From the three experimental sets of total pressure, the one reported by Kuranov et al.
 607 showed the lowest deviations for both cases. Similar observations were made also by
 608 Huttenhuis et al. [20] during the evaluation of their model developed for the H₂S-MDEA-H₂O
 609 system. Although the model framework they used (electrolyte EoS for both phases) differs from
 610 ours, their model predictions also showed highest deviations for the data from MacGregor and
 611 Mather and lowest for the data from Maddox et al. [27] and Kuranov et al. [17]. **Figure 10**
 612 shows experimental and modelled values for a 50 wt.% aqueous MDEA system as a function
 613 of temperature in Case B.



614

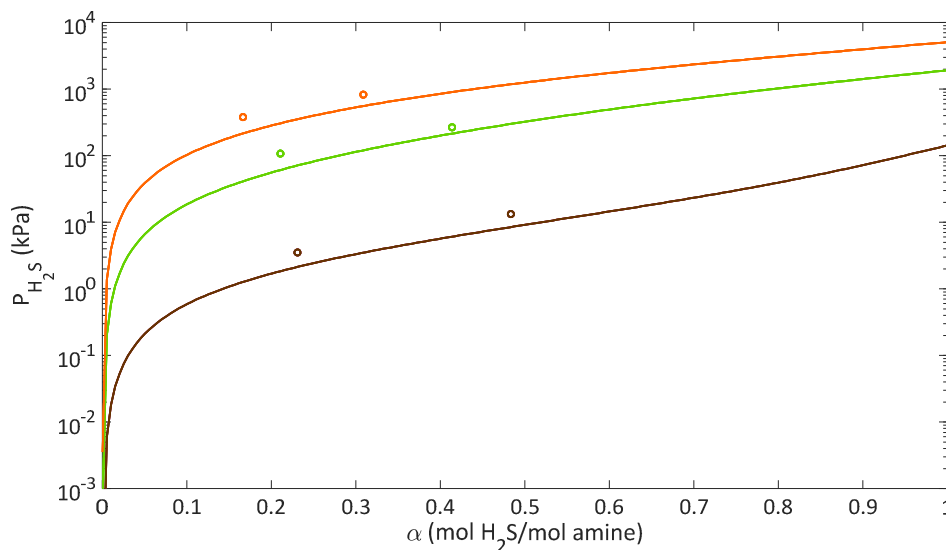
615 **Figure 10:** Hydrogen sulfide loading for 50 wt.% MDEA-H₂O as a function of partial pressure
 616 and temperature; (red) 313 K, (green) 343 K, (blue) 373 K, (orange) 393 K; (—) model, □
 617 Huang and Ng [23], Δ Rogers et al. [24] (1998), □ Jou et al. [21] (1993). Regression in Case B.

618 The differences in H_2S partial pressure noticed in the literature data as well as in our data
 619 obtained in the presence of methane for relatively low total pressure levels, are comparable to
 620 the accuracy of the model. Therefore, since also the effect of methane in the liquid loading has
 621 been found to be negligible for a 70 wt.% MDEA- H_2O , we also fitted the model to data available
 622 in the presence of methane. However, the code was not modified but, instead, the data for partial
 623 pressure of H_2S and loading were used as if methane was not present. Only data with maximum
 624 total pressure of 2000 kPa were considered, due to the more significant P_{H_2S} deviations
 625 observed at higher pressures in the literature for a 50 wt.% aqueous MDEA (Case C). To sum
 626 up, three cases were studied:

627 Case A. Regression of all available data in the absence of methane.

628 Case B. Regression of all available data in the absence of methane and loadings $\alpha > 0.05$
 629 mol H_2S /mol MDEA.

630 Case C. Regression of all available data in the absence of methane and loadings $\alpha > 0.05$
 631 mol H_2S /mol MDEA, and the data in the presence of methane, loadings $\alpha > 0.05$ mol H_2S /mol
 632 MDEA and maximum total pressures P_{tot} of 2000 kPa.



633

634 **Figure 11:** Hydrogen sulfide loading for 70 wt.% MDEA- H_2O as a function of partial pressure
 635 and temperature; (brown) 283 K, (green) 353 K, (orange) 393 K; (—) model, \circ This work.
 636 Regression in Case C.

637

638 **Table 13:** BIAS^a, AADs^b and AARDs^c for the fitted total pressures, P_{tot} , and H₂S partial pressures, $P_{\text{H}_2\text{S}}$, for Cases A, B and C.

| Source | Case A | | | | Case B | | | | Case C | | | |
|----------------------------|--|--------------|--------------|-------------|----------------|--------------|--------------|-------------|----------------|--------------|--------------|-------------|
| | Pressure range | Bias | AAD | AARD | Pressure range | Bias | AAD | AARD | Pressure range | Bias | AAD | AARD |
| | kPa | (%) | kPa | (%) | kPa | (%) | kPa | (%) | kPa | (%) | kPa | (%) |
| | Partial pressure, $P_{\text{H}_2\text{S}}$ | | | | | | | | | | | |
| Lemoine et al. [28] | 0.023-1.611 | -42.8 | 0.1 | 42.8 | 0.176-1.611 | -27.0 | 0.2 | 27.0 | 0.176-1.611 | -23.7 | 0.1 | 23.7 |
| Huang and Ng [23] | 0.0033-3673 | -32.7 | 80.4 | 38.8 | 2.34-3673 | -5.0 | 82.9 | 8.6 | 2.34-3673 | -2.5 | 69.0 | 13.3 |
| Rogers et al. [24] | 0.00069-5.268 | -25.7 | 0.1 | 32.2 | 0.2-5.268 | -12.1 | 0.2 | 13.0 | 0.2-5.268 | -6.8 | 0.2 | 12.3 |
| MacGregor and Mather [14] | 0.52-1600 | 48.4 | 19.3 | 48.7 | 0.52-1600 | 36.6 | 11.5 | 37.7 | 0.52-1600 | 49.0 | 15.8 | 49.2 |
| Jou et al. [21] | 0.00183-313 | -8.1 | 5.9 | 23.6 | 0.295-313 | -2.0 | 3.6 | 13.0 | 0.295-313 | 6.1 | 5.9 | 13.4 |
| Jou et al. [12] | 0.0013-5890 | 18.2 | 125.6 | 29.7 | 0.0273-5890 | 9.5 | 109.7 | 17.6 | 0.0273-5890 | 13.9 | 105.7 | 20.6 |
| Zoghi and Shokouhi [22] | 28-1361 | 24.2 | 42.4 | 26.2 | 14-1361 | 14.4 | 32.1 | 16.4 | 14-1361 | 20.4 | 36.5 | 22.2 |
| Maddox et al. [27] | 13.23-1536.6 | -4.9 | 74.8 | 15.2 | 13.23-1536.6 | -8.5 | 78.0 | 13.4 | 13.23-1536.6 | -6.4 | 77.1 | 13.9 |
| Huttenhuis et al. [25] | | | | - | | | | - | 0.141-1.495 | -35.0 | 0.3 | 35.0 |
| Dicko et al. [29] | | | | - | | | | - | 3-278 | -17.0 | 11.6 | 17.0 |
| Sadegh et al. [30] | | | | - | | | | - | 53-386 | -10.9 | 11.4 | 10.9 |
| This work | | | | - | | | | - | 2.60-818.12 | -20.2 | 36.5 | 21.3 |
| Overall | | 0.9 | 70.4 | 30.4 | | 3.5 | 66.2 | 17.8 | | 5.1 | 58.4 | 20.6 |
| | Total pressure, P_{tot} | | | | | | | | | | | |
| Kuranov et al. [17] | 165.2-4895.9 | -9.6 | 240.3 | 12.5 | 165.2-4895.9 | -10.5 | 241.1 | 13.6 | 165.2-4895.9 | -10.0 | 241.5 | 12.9 |
| Kamps et al. [18] | 147.9-2783 | -15.2 | 213.7 | 16.0 | 147.9-2783 | -20.8 | 231.5 | 20.8 | 147.9-2783 | -13.7 | 173.5 | 14.2 |
| Sidi-Boumedine et al. [19] | 6.21-1040 | -10.8 | 55.4 | 12.6 | 6.21-1040 | -16.4 | 70.3 | 16.7 | 6.21-1040 | -9.9 | 56.2 | 11.0 |
| Overall | | -11.0 | 194.4 | 13.2 | | -13.9 | 202.9 | 15.8 | | -10.8 | 187.9 | 12.7 |

639

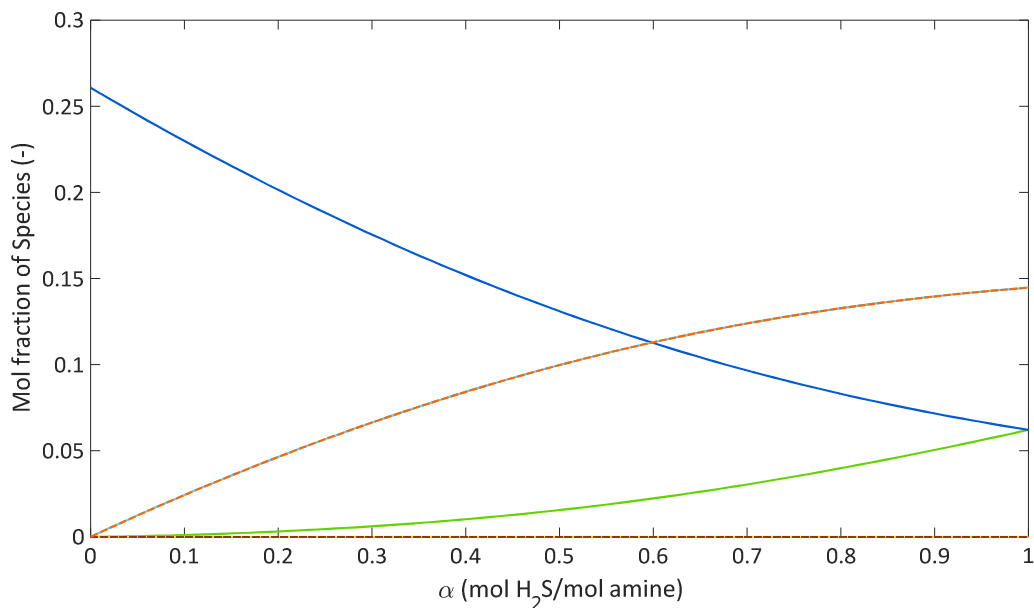
$${}^a\text{BIAS (\%)} = \frac{1}{N} \sum \frac{P_s^{pred} - P_s^{exp}}{P_s^{exp}} \cdot 100, {}^b\text{AAD} = \frac{1}{N} \sum |P_s^{pred} - P_s^{exp}|, {}^c\text{AARD (\%)} = \frac{1}{N} \sum \left| \frac{P_s^{pred} - P_s^{exp}}{P_s^{exp}} \right| \cdot 100$$

640

641 The model parameters obtained from the data regression in each case studied are given in
642 Supplementary Information. **Figure 11** shows experimental and modelled values for a 70 wt.%
643 aqueous MDEA system as a function of temperature in Case C while **Table 13** contains
644 information about each regression in terms of Bias, AADs and AARDs. The performance of
645 the model for a 70 wt% MDEA-H₂O system is good, especially considering the few data
646 available for this solvent concentration. In **Table 13**, it can be seen that the accuracy of the
647 model does not significantly change upon the addition of the experimental points with methane
648 in the regression. The overall AARD for the partial pressure is altered from 18% to 21%, which
649 is also the AARD calculated for the data published in this work. The data from MacGregor and
650 Mather [14] exhibit again the highest deviations while the measurements reported by Sadegh et
651 al. [30] in total pressure of 1500 kPa with methane as makeup gas show the lowest deviation,
652 11%. The slight deterioration of the fitting for the equilibrium H₂S can be also attributed to the
653 fact that experimental points obtained for high amine concentrations are used, i.e. 70 wt.% in
654 this work, but it can also be the result of the sensitivity of the algorithm to the numerical method.
655 To illustrate the latter, we repeated the data regression for Case A. The resulted AARDs were
656 29.8% and 30.1%, using the exact same data and fixed parameters. As far as the ability of the
657 model to predict the total pressure is concerned, the accuracy has surprisingly improved. This
658 is merely a lucky coincidence due to the fitting of the experimental points for methane-included
659 systems.

660 Speciation information is necessary in the development of process models for the accurate
661 design and operation of gas processing plants. Speciation results, calculated with the model
662 presented in this work, are provided in **Figure 12** where mole fractions of all the species in the
663 liquid phase are plotted against liquid loading for 70 wt.% aqueous MDEA at 353 K. It is shown
664 that as the loading increases, the concentration of MDEA declines and the concentration of
665 protonated amine MDEAH⁺ increases. At loadings close to 1, most of the amine has been
666 protonated and the mole fractions of MDEA and H₂S are equal. The curves representing
667 MDEAH⁺ and HS⁻ overlap, a behavior expected since the formation of sulfide was not taken
668 into account due to its low concentration, therefore the amount of HS⁻ and MDEAH⁺ formed
669 are balanced. H₃O⁺ and OH⁻ also overlap and they are practically zero throughout the loading
670 range. No experimental data were found for the speciation distribution in the H₂S-MDEA-H₂O
671 system to confirm the model predictions. Speciation graphs for 50.1 wt.% and 70 wt.% MDEA-
672 H₂O at the temperatures studied in this work are provided in Supplementary Information.

673



674

675 **Figure 12:** Predicted speciation of H₂S, MDEA and H₂O in 70 wt.% MDEA-H₂O at 353 K. (—)
 676 H₂S, (—) MDEA, (—) H₂O, (—) MDEAH⁺, (---) OH⁻, (---) HS⁻.

677

678 Overall, although the model developed in this work contains MDEA, H₂O, H₂S and the
 679 relevant ionic species, it can predict vapor-liquid equilibria for systems containing methane at
 680 low total pressures with similar accuracy as the systems in the absence of methane. However,
 681 it is recommended to be used only for rough estimations for H₂S-CH₄-MDEA-H₂O system and
 682 a model taking into account the methane solubility to be used if available. This model should
 683 not be used for systems with total pressure higher than 2000 kPa, where the gas fugacities
 684 change substantially.

685 6. Conclusions

686 Experimental vapor-liquid equilibrium data were measured for a 50.1 wt.% aqueous MDEA
 687 at temperature of 323 K and pressure up to 3000 kPa as well as a 70 wt.% aqueous MDEA at
 688 temperature of 283 K, 353 K and 323 K and pressures up to 10000 kPa, due to their relevance
 689 for subsea H₂S removal of natural gas. Therefore, methane was used as makeup gas. The
 690 experimental data indicate that the effect of total pressure on the liquid loading of the solvent
 691 is within the experimental uncertainties, while for the 50 wt.% MDEA-H₂O system the impact
 692 on the partial pressure of hydrogen sulfide is attributed to the non-idealities of the vapor phase
 693 and it is lower with decreasing total pressure. The system H₂S-MDEA-H₂O up to 70 wt.%

694 MDEA was modeled employing Peng-Robinson EoS to describe the vapor phase and eNRTL
695 activity coefficient model for the liquid phase. The AARD for the partial pressure of H₂S and
696 for the total system pressure was found to be 18% and 16% respectively. The effect of including
697 data in the presence of methane and maximum total pressure of 2000 kPa in the data regression
698 was studied and found minimal. However, for higher total pressure and different conditions
699 than the studied ones, the use of models taking into account the methane presence was
700 suggested. Last but not least, new parameters for Antoine correlation were proposed for the
701 estimation of the vapor pressure of MDEA based on our new measurements and all available
702 literature data covering a wide temperature range.

703

704 **Acknowledgements**

705 The authors acknowledge the valuable help from Mr. Eric Boonaert and Ing. Alain Valtz during
706 the laboratory work with the high-pressure VLE apparatus. Anastasia A. Trollebø is
707 acknowledged for conducting the pure MDEA saturation pressure measurements and Ricardo
708 R. Wanderley for the insightful discussions.

709

710 **Funding**

711 This work was supported by the Norwegian University of Science and Technology (NTNU),
712 major industry partners and the Research Council of Norway (RCN) [project number 237893].
713 It was carried out as a part of SUBPRO (Subsea Production and Processing), a Research-based
714 Innovation Centre within Subsea Production and Processing.

715

716 **List of Symbols**

| | | |
|-----|------------|---|
| 717 | <i>a</i> | parameter of Eq. 10 |
| 718 | A_{ϕ} | Debye-Hückel parameter |
| 719 | <i>b</i> | parameter of Eq. 10 |
| 720 | <i>c-a</i> | cation-anion |
| 721 | <i>D</i> | Dielectric constant (-) |
| 722 | g^{ex} | Molar excess Gibbs energy (J/mol) |
| 723 | <i>G</i> | eNRTL auxiliary function (-) |
| 724 | <i>H</i> | Henry's constant (kPa m ³ /kmol) |

| | | |
|-----|----------------------|---|
| 725 | I_x | Ionic strength in mole fraction scale (mol/m ³) |
| 726 | k | Boltzmann constant (J/K) |
| 727 | m | molecule |
| 728 | M | Molecular weight (kg/kmol) |
| 729 | N_A | Avogadro number (mol ⁻¹) |
| 730 | P | Pressure (kPa) |
| 731 | r_{BORN} | Born radius (m) |
| 732 | R | Gas constant (J mol ⁻¹ K ⁻¹) |
| 733 | T | Absolute temperature (K) |
| 734 | v | Molar volume (m ³ /mol) |
| 735 | w | Weight fraction (-) |
| 736 | x | Mole fraction (-) |
| 737 | X | eNRTL mole fraction (-) |
| 738 | z | Ionic charge (-) |
| 739 | Z | Absolute value of the ionic charge (-) |
| 740 | | |
| 741 | Greek letters | |
| 742 | α | Loading (mol H ₂ S/mol MDEA) |
| 743 | γ | Activity coefficient (-) |
| 744 | ε | Permittivity (F/m) |
| 745 | ρ | Molar density (mol/cm ³) |
| 746 | ρ_{pdh} | Closest approach parameter of the Pitzer-Debye-Hückel formulation (-) |
| 747 | τ | Energy parameter (-) |
| 748 | | |
| 749 | Superscripts | |
| 750 | E | Excess property |
| 751 | exp | Experimental value |
| 752 | l | Liquid phase |
| 753 | lc | Local composition |

| | | |
|-----|----------------------|--|
| 754 | pdh | Pitzer-Debye-Hückel formulation |
| 755 | phys | Physical absorption |
| 756 | pred | Predicted value |
| 757 | v | Vapor phase |
| 758 | | |
| 759 | Subscripts | |
| 760 | amb | Ambient |
| 761 | app | Apparent |
| 762 | aq, MDEA | Aqueous MDEA |
| 763 | c | Critical |
| 764 | glob | Global, refers to global loading α_{glob} (mol H ₂ S in the cell/mol MDEA) |
| 765 | i, j, k | Component in a mixture |
| 766 | ij | Cross parameter |
| 767 | liq | Liquid, refers to liquid loading α_{liq} (mol H ₂ S/mol MDEA) |
| 768 | s | solvent |
| 769 | w | water |
| 770 | | |
| 771 | Abbreviations | |
| 772 | AAD | Average Absolute Deviation |
| 773 | AARD | Average Absolute Relative Deviation |
| 774 | eNRTL | electrolyte Non-Random Two Liquids |
| 775 | EoS | Equation of State |
| 776 | FPD | Freezing Point Depression |
| 777 | FTIR | Fourier-Transform infrared |
| 778 | GC | Gas Chromatography |
| 779 | MDEA | Methyldiethanolamine |
| 780 | NP | Number of data points |
| 781 | NS | Number of vapor phase samples for GC analysis |
| 782 | VLE | Vapor-Liquid Equilibrium |

784 **Appendix A: eNRTL model**

785 The activity coefficients were calculated by the electrolyte Non-Random Two Liquids (eNRTL)
786 model [50]:

787 The starting point for the description of the liquid phase is the expression of excess Gibbs
788 energy as the sum of two terms; one related to the long-range forces between the ions (first
789 term) and one to the short-range forces between all the species (second term):

$$\frac{g^E}{RT} = \frac{g^{E,pdh}}{RT} + \frac{g^{E,lc}}{RT} \quad \text{Eq. A1}$$

790 This equation lead to:

$$\ln \gamma_i = \ln \gamma_i^{pdh} + \ln \gamma_i^{lc} \quad \text{Eq. A2}$$

791 The subscript *pdh* denotes Pitzer-Debye-Hückel formulation for the long-range interactions and
792 the subscript *lc* denotes Local Composition model. The formulation of the former is:

$$\frac{g^{E,pdh}}{RT} = - \left(\sum_k x_k \right) \left(\frac{1000}{M_s} \right)^{\frac{1}{2}} \left(\frac{4A_\phi I_x}{\rho_{pdh}} \right) \ln(1 + \rho_{pdh} I_x^{\frac{1}{2}}) \quad \text{Eq. A3}$$

793 By derivation, the activity coefficient is expressed according to:

$$\begin{aligned} \ln \gamma_i^{*pdh} = & - (1000/M_s)^{\frac{1}{2}} A_\phi \left[\left(2 \frac{Z_i^2}{\rho_{pdh}} \right) \ln \left(1 + \rho_{pdh} I_x^{\frac{1}{2}} \right) \right. \\ & \left. + \left(Z_i^2 I_x^{\frac{1}{2}} - 2 I_x^{\frac{3}{2}} \right) / (1 + \rho_{pdh} I_x^{\frac{1}{2}}) \right] \end{aligned} \quad \text{Eq. A4}$$

794 where I_x is the ionic strength and A_ϕ is the Debye-Hückel parameter, expressed as following:

$$I_x = \frac{1}{2} \sum_i Z_i^2 x_i, \quad A_\phi = \frac{1}{3} \left(\frac{2\pi N_o d}{1000} \right)^{\frac{1}{2}} \left(\frac{e^2}{DkT} \right)^{3/2} \quad \text{Eq. A5}$$

795 The reference state for the *pdh* term is infinite dilution in the mixed solvent while the reference
796 state for the *lc* term is infinite dilution in water. To account for the excess Gibbs energy of
797 transfer from the infinite dilution in the mixed solvent to the infinite dilution in water, a term is
798 added in the long-range interaction expression. This additional term is described by the Born
799 equation:

$$\frac{g^{E,BORN}}{RT} = - \frac{N_A e^2}{8\pi R T r_{BORN} \epsilon_o} \left(\frac{1}{\epsilon_s} - \frac{1}{\epsilon_w} \right) \sum_i x_i z_i^2 \quad \text{Eq. A6}$$

800 Further,

$$\ln \gamma_i^{BORN} = \frac{N_A e^2}{8\pi R T r_{BORN} \epsilon_o} \left(\frac{1}{\epsilon_s} - \frac{1}{\epsilon_w} \right) z_i^2 \quad \text{Eq. A7}$$

801

802 The short-range contribution is described by the eNRTL model as following:

$$\begin{aligned} \frac{g^{E,lc}}{RT} = & \sum_m X_m \frac{\sum_j X_j G_{jm} \tau_{jm}}{\sum_k X_k G_{km}} + \sum_c X_c \sum_{a'} \frac{X_{a'}}{\sum_k X_k G_{km}} \frac{\sum_j X_j G_{jc,a'c} \tau_{jc,a'c}}{\sum_k X_k G_{kc,a'c}} \\ & + \sum_a X_a \sum_{c'} \frac{X_{c'}}{\sum_{c''} X_{c''}} \frac{\sum_j X_j G_{ja,c'a} \tau_{ja,c'a}}{\sum_k X_k G_{ka,c'a}} \end{aligned} \quad \text{Eq. A8}$$

803 where m , c and a denote molecule, cation and anion, while $X_j = C_j x_j$ with j : m , c , a effective
804 local mole fraction. Equations A9 and A10 are given using the ion-like repulsion assumption
805 and the local electroneutrality assumption.

$$G_{cm} = \frac{\sum_a X_a G_{ca,m}}{\sum_{a'} X_{a'}} \quad \text{Eq. A9}$$

$$G_{am} = \frac{\sum_c X_c G_{ca,m}}{\sum_{c'} X_{c'}} \quad \text{Eq. A10}$$

806 The $G_{i,j}$ and $\tau_{i,j}$ parameters are related through the non-randomness parameter, $a_{i,j}$:

$$G_{ij} = \exp(-a_{i,j} \tau_{i,j}) \quad \text{Eq. A11}$$

807 The equations presented below describe the non-randomness parameters:

$$a_{cm} = \frac{\sum_a X_a a_{ca,m}}{\sum_{a'} X_{a'}} \quad \text{Eq. A12}$$

$$a_{am} = \frac{\sum_c X_c a_{ca,m}}{\sum_{c'} X_{c'}} \quad \text{Eq. A13}$$

808 The energy parameters $\tau_{mc,ac}$ and $\tau_{ma,ca}$ are given by:

$$\tau_{mc,ac} = \tau_{cm} - \frac{a_{ca,m}}{a_{mc,ac}} (\tau_{ca,m} - \tau_{m,ca}) \quad \text{Eq. A14}$$

$$\tau_{ma,ca} = \tau_{am} - \frac{a_{ca,m}}{a_{ma,ca}} (\tau_{ca,m} - \tau_{m,ca}) \quad \text{Eq. A15}$$

809 where

$$a_{mc,ac} = a_{cm} \quad \text{Eq. A16}$$

$$a_{am,ac} = a_{am} \quad \text{Eq. A17}$$

810

811 The adjustable binary parameters are the non-randomness factors $a_{ca,m}$, $a_{ca,ca'}$, $a_{ca,c'a}$, $a_{mm'}$,
812 and the energy parameters $\tau_{ca,m}$, $\tau_{m,ca}$, $\tau_{ca,ca'}$, $\tau_{ca',ca}$, $\tau_{ca,c'a}$, $\tau_{c'a,ca}$, $\tau_{m,m'}$, $\tau_{m'm}$.

813

814 From Equation A8, the activity coefficients are calculated:

815 For molecules:

$$\begin{aligned} \ln \gamma_m^{lc} = & \frac{\sum_j X_j G_{jm} \tau_{jm}}{\sum_k X_k G_{km}} + \sum_{m'} \frac{X_{m'} G_{mm'}}{\sum_k X_k G_{km'}} \left(\tau_{mm'} - \frac{\sum_k X_k G_{km'} \tau_{km'}}{\sum_k X_k G_{km'}} \right) \\ & + \sum_c \sum_{a'} \frac{X_{a'}}{\sum_{a''} X_{a''}} \frac{X_{c'} G_{mc,a'c}}{\sum_k X_k G_{kc,a'c}} \left(\tau_{mc,a'c} - \frac{\sum_k X_k G_{kc,a'c} \tau_{kc,a'c}}{\sum_k X_k G_{kc,a'c}} \right) \\ & + \sum_a \sum_{c'} \frac{X_{c'}}{\sum_{c''} X_{c''}} \frac{X_{a'} G_{ma,c'a}}{\sum_k X_k G_{ka,c'a}} \left(\tau_{ma,c'a} - \frac{\sum_k X_k G_{ka,c'a} \tau_{ka,c'a}}{\sum_k X_k G_{ka,c'a}} \right) \end{aligned}$$

Eq. A18

816

817 For cations:

$$\begin{aligned} \frac{1}{Z_c} \ln \gamma_c^{lc} = & \sum_{a'} \frac{X_{a'}}{\sum_{a''} X_{a''}} \frac{\sum_k X_k G_{kc,a'c} \tau_{kc,a'c}}{\sum_k X_k G_{kc,a'c}} \\ & + \sum_m \frac{X_m G_{cm}}{\sum_k X_k G_{km}} \left(\tau_{cm} - \frac{\sum_k X_k G_{km} \tau_{km}}{\sum_k X_k G_{km}} \right) \\ & + \sum_a \sum_{c'} \frac{X_{c'}}{\sum_{c''} X_{c''}} \frac{X_{a'} G_{ca,c'a}}{\sum_k X_k G_{ka,c'a}} \left(\tau_{ca,c'a} - \frac{\sum_k X_k G_{ka,c'a} \tau_{ka,c'a}}{\sum_k X_k G_{ka,c'a}} \right) \end{aligned}$$

Eq. A19

818

819 For anions:

$$\begin{aligned}
\frac{1}{Z_a} \ln \gamma_a^{lc} = & \sum_{c'} \frac{X_{c'}}{\sum_{c''} X_{c''}} \frac{\sum_k X_k G_{ka,c'a} \tau_{ka,c'a}}{\sum_k X_k G_{ka,c'a}} \\
& + \sum_m \frac{X_m G_{am}}{\sum_k X_k G_{km}} \left(\tau_{am} - \frac{\sum_k X_k G_{km} \tau_{km}}{\sum_k X_k G_{km}} \right) \\
& + \sum_c \sum_{a'} \frac{X_{a'}}{\sum_{a''} X_{a''}} \frac{X_c G_{ac,a'c}}{\sum_k X_k G_{kc,a'c}} \left(\tau_{ac,a'c} - \frac{\sum_k X_k G_{kc,a'c} \tau_{kc,a'c}}{\sum_k X_k G_{kc,a'c}} \right)
\end{aligned}$$

Eq. A20

820

821 The expressions of activity coefficients at infinite dilution are then:

$$\ln \gamma_m^{lc,\infty} = \tau_{wm} + G_{mw} \tau_{mw} \quad \text{Eq. A21}$$

$$\frac{1}{Z_c} \ln \gamma_c^{lc,\infty} = \frac{X_a}{\sum_{a'} X_{a'}} \tau_{wc,ac} + G_{cw} \tau_{cw} \quad \text{Eq. A22}$$

$$\frac{1}{Z_a} \ln \gamma_a^{lc,\infty} = \frac{X_c}{\sum_{c'} X_{c'}} \tau_{wa,ca} + G_{aw} \tau_{aw} \quad \text{Eq. A23}$$

822 By combination of Equations A2, A4, A7, A18 and A23, the activity coefficient for the liquid
823 phase is found by:

$$\gamma_i = \gamma_i^{pdh} \gamma_i^{BORN} \gamma_i^{lc} / \gamma_i^{lc,\infty} \quad \text{Eq. A24}$$

824 where $i = m, c$ or a for all components, besides the amine in this work. For MDEA, the
825 symmetric reference state for the short-range interactions contribution, $\gamma_{MDEA}^{lc,\infty}$ is fixed to 1.

826 **Appendix B:** Peng-Robinson Equation of State

827 The fugacity coefficients were calculated by Peng-Robinson equation of state [49]:

$$P = \frac{RT}{v-b} - \frac{\alpha a(T)}{v^2 + 2bv - b^2} \quad \text{Eq. A25}$$

828 where:

$$a = 0.42724 \frac{R^2 T_c^2}{P_c}, \quad b = 0.07780 \frac{RT_c}{P_c}, \quad a(T) = \left[1 + m \left(1 - T_R^{\frac{1}{2}} \right) \right]^2 \quad \&$$

$$m = 0.37464 + 1.54226\omega - 2.26992\omega^2$$

829

830 The traditional van der Waals one-fluid mixing rules were used for the estimation of the gas
831 mixture parameters from the pure components' properties.

$$a(T) = \sum_i \sum_j x_i x_j (a(T))_i^{\frac{1}{2}} (a(T))_j^{\frac{1}{2}} (1 - k_{ij}) \quad \& \quad b = \sum_i x_i b_i$$

832 In our work, the binary interaction parameter k_{ij} is set to zero, so as the eNRTL model
833 parameters are the only ones fitted.

834 The critical properties used in this work can be found in Supporting Information.

835 **Appendix C: Supplementary Information**

836 Supplementary information includes:

837 A. Critical properties and acentric factors for pure components

838 B. Model parametrization

839 C. Modeling results

840 D. Experimental results

841 E. Uncertainty analysis

842 **References**

- 843 [1] G. Astarita, D. W. Savage, and A. Bisio, *Gas treating with chemical solvents*. New
844 York, United States: John Wiley, 1983.
- 845 [2] J. M. Campbell, "Amine-based processes," in *Gas Conditioning and Processing*, vol. 4,
846 Oklahoma, USA, 1998.
- 847 [3] A. L. Kohl and R. B. Nielsen, "Chapter 2 - Alkanolamines for Hydrogen Sulfide and
848 Carbon Dioxide Removal," in *Gas Purification*, 5th ed., Houston: Gulf Professional
849 Publishing, 1997, pp. 40–186.
- 850 [4] Z. I. Khatib and J. R. Salanitro, "Reservoir Souring: Analysis of Surveys and Experience
851 in Sour Waterfloods," presented at the SPE Annual Technical Conference and
852 Exhibition, 1997, doi: 10.2118/38795-MS.
- 853 [5] A. F. Mitchell and S. Asa, "10248: A REVIEW OF RESERVOIR SOURING FOR
854 THREE NORTH SEA FIELDS.," p. 8.
- 855 [6] GATEkeeper, "H2S scavenging: Using Triazine," May-2014.
- 856 [7] O. Økland, S. Davies, R. M. Ramberg, and H. Rognø, "Steps to the Subsea Factory," in
857 *OTC-24307-MS*, OTC, 2013, doi: 10.4043/24307-MS.
- 858 [8] M. Davoudi, Y. Heidari, A. Safadoost, and S. Samieirad, "Chemical injection policy for
859 internal corrosion prevention of South Pars sea-pipeline: A case study," *Journal of*

- 860 *Natural Gas Science and Engineering*, vol. 21, pp. 592–599, Nov. 2014, doi:
861 10.1016/j.jngse.2014.09.017.
- 862 [9] “UWP/Subsea on a Stick®,” *Kvaerner - UWP/Subsea on a Stick®*. [Online]. Available:
863 <https://www.kvaerner.com/Products/Subsea-on-a-Stick/>. [Accessed: 13-Mar-2019].
- 864 [10] J. Addicks, G. A. Owren, A. O. Fredheim, and K. Tangvik, “Solubility of Carbon
865 Dioxide and Methane in Aqueous Methyldiethanolamine Solutions,” *J. Chem. Eng.*
866 *Data*, vol. 47, no. 4, pp. 855–860, Jul. 2002, doi: 10.1021/je010292z.
- 867 [11] Ø. Jonassen, *Equilibrium and thermal properties of selected CO₂-methane-tertiary*
868 *amine systems; an experimental and modelling study*. NTNU, 2017.
- 869 [12] F. Y. Jou, A. E. Mather, and F. D. Otto, “Solubility of hydrogen sulfide and carbon
870 dioxide in aqueous methyldiethanolamine solutions,” *Ind. Eng. Chem. Proc. Des. Dev.*,
871 vol. 21, no. 4, pp. 539–544, Oct. 1982, doi: 10.1021/i200019a001.
- 872 [13] M. H. Li and K. P. Shen, “Solubility of hydrogen sulfide in aqueous mixtures of
873 monoethanolamine with N-methyldiethanolamine,” *J. Chem. Eng. Data*, vol. 38, no. 1,
874 pp. 105–108, Jan. 1993, doi: 10.1021/je00009a025.
- 875 [14] R. J. MacGregor and A. E. Mather, “Equilibrium Solubility of H₂S and CO₂ and Their
876 Mixtures in a Mixed Solvent,” *Can. J. Chem. Eng.*, vol. 69, no. 6, pp. 1357–1366, Dec.
877 1991, doi: 10.1002/cjce.5450690618.
- 878 [15] J. M. Bernal-García, M. Ramos-Estrada, G. A. Iglesias-Silva, and K. R. Hall, “Densities
879 and Excess Molar Volumes of Aqueous Solutions of n-Methyldiethanolamine (MDEA)
880 at Temperatures from (283.15 to 363.15) K,” *J. Chem. Eng. Data*, vol. 48, no. 6, pp.
881 1442–1445, Nov. 2003, doi: 10.1021/je030120x.
- 882 [16] L. Chunxi and W. Fürst, “Representation of CO₂ and H₂S solubility in aqueous MDEA
883 solutions using an electrolyte equation of state,” *Chemical Engineering Science*, vol. 55,
884 no. 15, pp. 2975–2988, Aug. 2000, doi: 10.1016/S0009-2509(99)00550-3.
- 885 [17] G. Kuranov, B. Rumpf, N. A. Smirnova, and G. Maurer, “Solubility of Single Gases
886 Carbon Dioxide and Hydrogen Sulfide in Aqueous Solutions of N-
887 Methyldiethanolamine in the Temperature Range 313–413 K at Pressures up to 5 MPa,”
888 *Ind. Eng. Chem. Res.*, vol. 35, no. 6, pp. 1959–1966, Jan. 1996, doi: 10.1021/ie950538r.
- 889 [18] Á. P.-S. Kamps, A. Balaban, M. Jödecke, G. Kuranov, N. A. Smirnova, and G. Maurer,
890 “Solubility of Single Gases Carbon Dioxide and Hydrogen Sulfide in Aqueous Solutions
891 of N-Methyldiethanolamine at Temperatures from 313 to 393 K and Pressures up to 7.6
892 MPa: New Experimental Data and Model Extension,” *Ind. Eng. Chem. Res.*, vol. 40, no.
893 2, pp. 696–706, Jan. 2001, doi: 10.1021/ie000441r.
- 894 [19] R. Sidi-Boumedine, S. Horstmann, K. Fischer, E. Provost, W. Fürst, and J. Gmehling,
895 “Experimental determination of hydrogen sulfide solubility data in aqueous
896 alkanolamine solutions,” *Fluid Phase Equilibria*, vol. 218, no. 1, pp. 149–155, Apr.
897 2004, doi: 10.1016/j.fluid.2003.11.020.
- 898 [20] P. J. G. Huttenhuis, N. J. Agrawal, and G. F. Versteeg, “The solubility of hydrogen
899 sulfide in aqueous N-methyldiethanolamine solutions,” *Int. J. Oil, Gas and Coal*
900 *Technology*, vol. 1, no. 4, pp. 399–424, 2008.
- 901 [21] F.-Y. Jou, J. J. Carroll, A. E. Mather, and F. D. Otto, “The solubility of carbon dioxide
902 and hydrogen sulfide in a 35 wt% aqueous solution of methyldiethanolamine,” *Can. J.*
903 *Chem. Eng.*, vol. 71, no. 2, pp. 264–268, Apr. 1993, doi: 10.1002/cjce.5450710213.
- 904 [22] A. T. Zoghi and M. Shokouhi, “Measuring solubility of hydrogen sulphide in aqueous
905 blends of N-methyldiethanolamine and 2-((2 aminoethyl)amino)ethanol and correlating
906 by the Deshmukh-Mather model,” *Journal of Chemical Thermodynamics*, vol. 100, pp.
907 106–115, 2016, doi: 10.1016/j.jct.2016.04.012.
- 908 [23] S. H. Huang and H.-J. Ng, “Solubility of H₂S and CO₂ in Alkanolamines,” *Gas*
909 *Processors Association*, RR-155, Sep. 1998.

- 910 [24] W. J. Rogers, J. A. Bullin, and R. R. Davison, "FTIR measurements of acid-gas -
911 Methyl-diethanolamine systems," *AIChE Journal*, vol. 44, no. 11, pp. 2423–2430, 1998.
- 912 [25] P. J. G. Huttenhuis, N. J. Agrawal, J. A. Hogendoorn, and G. F. Versteeg, "Gas
913 solubility of H₂S and CO₂ in aqueous solutions of N-methyl-diethanolamine," *Journal of*
914 *Petroleum Science and Engineering*, vol. 55, no. 1, pp. 122–134, Jan. 2007, doi:
915 10.1016/j.petrol.2006.04.018.
- 916 [26] A. M. Bhairi, "Experimental Equilibrium Between Acid Gases and Ethanolamine
917 Solutions," Jul. 1984.
- 918 [27] R. N. Maddox, A. H. Bhairi, J. R. Diers, and P. A. Thomas, "Equilibrium solubility of
919 carbon dioxide or hydrogen sulfide in aqueous solutions of monoethanolamine,
920 diglycolamine, diethanolamine and methyl-diethanolamine: project 841," Gas Processors
921 Association, Tulsa, Okla, RR-104, 1987.
- 922 [28] B. Lemoine, Y.-G. Li, R. Cadours, C. Bouallou, and D. Richon, "Partial vapor pressure
923 of CO₂ and H₂S over aqueous methyl-diethanolamine solutions," *Fluid Phase*
924 *Equilibria*, vol. 172, no. 2, pp. 261–277, Jul. 2000, doi: 10.1016/S0378-3812(00)00383-
925 6.
- 926 [29] M. Dicko, C. Coquelet, C. Jarne, S. Northrop, and D. Richon, "Acid gases partial
927 pressures above a 50 wt% aqueous methyl-diethanolamine solution: Experimental work
928 and modeling," *Fluid Phase Equilibria*, vol. 289, no. 2, pp. 99–109, Mar. 2010, doi:
929 10.1016/j.fluid.2009.11.012.
- 930 [30] N. Sadegh, K. Thomsen, E. Solbraa, E. Johannessen, G. I. Rudolfsen, and O. J. Berg,
931 "Solubility of hydrogen sulfide in aqueous solutions of N-methyl-diethanolamine at high
932 pressures," *Fluid Phase Equilibria*, vol. 393, pp. 33–39, May 2015, doi:
933 10.1016/j.fluid.2015.02.016.
- 934 [31] H. T. Chang, M. Posey, and G. T. Rochelle, "Thermodynamics of alkanolamine-water
935 solutions from freezing point measurements," *Industrial & engineering chemistry*
936 *research*, vol. 32, no. 10, pp. 2324–2335, 1993.
- 937 [32] P. L. Fosbøl, M. G. Pedersen, and K. Thomsen, "Freezing Point Depressions of Aqueous
938 MEA, MDEA, and MEA–MDEA Measured with a New Apparatus," *J. Chem. Eng.*
939 *Data*, vol. 56, no. 4, pp. 995–1000, Apr. 2011, doi: 10.1021/je100994v.
- 940 [33] I. Kim, H. F. Svendsen, and E. Børresen, "Ebulliometric Determination of Vapor–Liquid
941 Equilibria for Pure Water, Monoethanolamine, N-Methyl-diethanolamine, 3-
942 (Methylamino)-propylamine, and Their Binary and Ternary Solutions," *J. Chem. Eng.*
943 *Data*, vol. 53, no. 11, pp. 2521–2531, Nov. 2008, doi: 10.1021/je800290k.
- 944 [34] S. Xu, S. Qing, Z. Zhen, C. Zhang, and J. J. Carroll, "Vapor pressure measurements of
945 aqueous N-methyl-diethanolamine solutions," *Fluid Phase Equilibria*, vol. 67, pp. 197–
946 201, Nov. 1991, doi: 10.1016/0378-3812(91)90055-C.
- 947 [35] E. Voutsas, A. Vrachnos, and K. Magoulas, "Measurement and thermodynamic
948 modeling of the phase equilibrium of aqueous N-methyl-diethanolamine solutions," *Fluid*
949 *Phase Equilibria*, vol. 224, no. 2, pp. 193–197, Oct. 2004, doi:
950 10.1016/j.fluid.2004.05.012.
- 951 [36] M. L. Posey, "Thermodynamic model for acid gas loaded aqueous alkanolamine
952 solutions.," 1996.
- 953 [37] Y. Maham, A. E. Mather, and L. G. Hepler, "Excess Molar Enthalpies of (Water +
954 Alkanolamine) Systems and Some Thermodynamic Calculations," *J. Chem. Eng. Data*,
955 vol. 42, no. 5, pp. 988–992, Sep. 1997, doi: 10.1021/je960296h.
- 956 [38] Y. Maham, A. E. Mather, and C. Mathonat, "Excess properties of (alkyl-diethanolamine
957 +H₂O) mixtures at temperatures from (298.15 to 338.15) K," *The Journal of Chemical*
958 *Thermodynamics*, vol. 32, no. 2, pp. 229–236, Feb. 2000, doi: 10.1006/jcht.1999.0595.

- 959 [39] O. Noll, A. Valtz, D. Richon, T. Getachew-Sawaya, I. Mokbel, and J. Jose, "Vapor
960 pressures and liquid densities of N-methylethanolamine, diethanolamine, and N-
961 methyldiethanolamine," *ELDATA: Int. Electron. J. Phys.-Chem. Data*, vol. 4, pp. 105–
962 120, 1998.
- 963 [40] T. E. Daubert, J. W. Jalowka, and V. Goren, "Vapor pressure of 22 pure industrial
964 chemicals," in *AIChE Symp. Ser.*, 1987, vol. 83, pp. 128–156.
- 965 [41] C. Yang *et al.*, "Vapor–Liquid Equilibria for Three Binary Systems of N-
966 Methylethanolamine, N-Methyldiethanolamine, and Ethylene Glycol at P = (40.0, 30.0,
967 and 20.0) kPa," *J. Chem. Eng. Data*, vol. 58, no. 8, pp. 2272–2279, Aug. 2013, doi:
968 10.1021/je400373d.
- 969 [42] D. M. VonNiederhausern, G. M. Wilson, and N. F. Giles, "Critical Point and Vapor
970 Pressure Measurements for 17 Compounds by a Low Residence Time Flow Method," *J.*
971 *Chem. Eng. Data*, vol. 51, no. 6, pp. 1990–1995, Nov. 2006, doi: 10.1021/je060269j.
- 972 [43] J. M. S. Fonseca, R. Dohrn, and S. Peper, "High-pressure fluid-phase equilibria:
973 Experimental methods and systems investigated (2005–2008)," *Fluid Phase Equilibria*,
974 vol. 300, no. 1, pp. 1–69, Jan. 2011, doi: 10.1016/j.fluid.2010.09.017.
- 975 [44] ARMINES, "Procédé et Dispositif Pour Prélever Des Microéchantillons D'un Fluide
976 Sous Pression Contenu Dans Un Container," 2 853 414, 2003.
- 977 [45] E. W. Lemmon, I. H. Bell, M. L. Huber, and M. O. McLinden, *NIST Standard Reference*
978 *Database 23: Reference Fluid Thermodynamic and Transport Properties-REFPROP*.
979 Gaithersburg: National Institute of Standards and Technology, Standard Reference Data
980 Program, 2018.
- 981 [46] E. W. Lemmon and R. Span, "Short Fundamental Equations of State for 20 Industrial
982 Fluids," *J. Chem. Eng. Data*, vol. 51, no. 3, pp. 785–850, May 2006, doi:
983 10.1021/je050186n.
- 984 [47] J. G. M.-S. Monteiro, D. D. D. Pinto, S. A. H. Zaidy, A. Hartono, and H. F. Svendsen,
985 "VLE data and modelling of aqueous N,N-diethylethanolamine (DEEA) solutions,"
986 *International Journal of Greenhouse Gas Control*, vol. 19, pp. 432–440, Nov. 2013, doi:
987 10.1016/j.ijggc.2013.10.001.
- 988 [48] D. D. D. Pinto, J. G. M.-S. Monteiro, A. Bersås, T. Haug-Warberg, and H. F. Svendsen,
989 "eNRTL Parameter Fitting Procedure for Blended Amine Systems: MDEA-PZ Case
990 Study," *Energy Procedia*, vol. 37, pp. 1613–1620, Jan. 2013, doi:
991 10.1016/j.egypro.2013.06.037.
- 992 [49] D.-Y. Peng and D. B. Robinson, "A New Two-Constant Equation of State," *Ind. Eng.*
993 *Chem. Fund.*, vol. 15, no. 1, pp. 59–64, Feb. 1976, doi: 10.1021/i160057a011.
- 994 [50] C.-C. Chen and L. B. Evans, "A local composition model for the excess Gibbs energy of
995 aqueous electrolyte systems," *AIChE Journal*, vol. 32, no. 3, pp. 444–454, 1986, doi:
996 10.1002/aic.690320311.
- 997 [51] J. L. Oscarson, X. Chen, and R. M. Izatt, "A thermodynamically consistent model for the
998 prediction of solubilities and enthalpies of solution of acid gases in aqueous
999 alkanolamine solutions," Gas Processors Association, Tulsa, Oklahoma, RR-130, 1995.
- 1000 [52] T. J. Edwards, J. Newman, and J. M. Prausnitz, "Thermodynamics of Vapor-Liquid
1001 Equilibria for the Ammonia-Water System," *Industrial & Engineering Chemistry*
1002 *Fundamentals*, vol. 17, no. 4, pp. 264–269, Nov. 1978, doi: 10.1021/i160068a007.
- 1003 [53] DIPPR, "DIPPR chemical database. Design Institute for Physical Property Data
1004 American Institute of Chemical Engineers,," 2004. .
- 1005 [54] E. T. Hessen, T. Haug-Warberg, and H. F. Svendsen, "The refined e-NRTL model
1006 applied to CO₂–H₂O–alkanolamine systems," *Chemical Engineering Science*, vol. 65,
1007 no. 11, pp. 3638–3648, Jun. 2010, doi: 10.1016/j.ces.2010.03.010.

- 1008 [55] J. Kennedy and R. C. Eberhart, "Proceedings of IEEE international conference on neural
1009 networks," *Perth, Australia*, 1995.
- 1010 [56] S. Ghosh, S. Das, D. Kundu, K. Suresh, and A. Abraham, "Inter-particle communication
1011 and search-dynamics of lbest particle swarm optimizers: An analysis," *Inf. Sci.*, vol. 182,
1012 no. 1, pp. 156–168, Jan. 2012, doi: 10.1016/j.ins.2010.10.015.
- 1013 [57] D. D. D. Pinto, "CO2 capture solvents; modeling and experimental characterization,"
1014 Norwegian University of Science and Technology, 2014.
- 1015 [58] B. N. Taylor and C. E. Kuyatt, "NIST Guidelines for Evaluating and Expressing the
1016 Uncertainty of NIST Measurement Results. NIST Technical Note 1297." Physics
1017 Laboratory, National Institute of Standards and Technology, Sep-1994.
- 1018 [59] E. B. Rinker and O. C. Sandall, "Physical solubility of hydrogen sulfide in several
1019 aqueous solvents," *The Canadian Journal of Chemical Engineering*, vol. 78, no. 1, pp.
1020 232–236, Feb. 2000, doi: 10.1002/cjce.5450780130.
- 1021 [60] H. A. Al-Ghawas, D. P. Hagewiesche, G. Ruiz-Ibanez, and O. C. Sandall,
1022 "Physicochemical properties important for carbon dioxide absorption in aqueous
1023 methyldiethanolamine," *J. Chem. Eng. Data*, vol. 34, no. 4, pp. 385–391, Oct. 1989, doi:
1024 10.1021/je00058a004.
- 1025 [61] E. Álvarez, D. Gómez-Díaz, M. D. La Rubia, and J. M. Navaza, "Densities and
1026 Viscosities of Aqueous Ternary Mixtures of 2-(Methylamino)ethanol and 2-
1027 (Ethylamino)ethanol with Diethanolamine, Triethanolamine, N-Methyldiethanolamine,
1028 or 2-Amino-1-methyl-1-propanol from 298.15 to 323.15 K," *J. Chem. Eng. Data*, vol.
1029 51, no. 3, pp. 955–962, May 2006, doi: 10.1021/je050463q.
- 1030 [62] T. T. Teng, Y. Maham, L. G. Hepler, and A. E. Mather, "Viscosity of Aqueous Solutions
1031 of N-Methyldiethanolamine and of Diethanolamine," *J. Chem. Eng. Data*, vol. 39, no. 2,
1032 pp. 290–293, Apr. 1994, doi: 10.1021/je00014a021.
- 1033
- 1034
- 1035